Crosstalk between Proteasomal and Lysosomal Protein Degradation Pathway in EBV-Induced B-cell Lymphomas

Summary of Work

PRESIDENCY UNIVERSITY
KOLKATA

Chandrima Gain

Enrolment No.: PU/PHD/BIOS/2017/022
Registration No.: R-17RS18220100

Supervisor: Dr. Abhik Saha

Tumor Virology Lab
School of Biotechnology
Presidency University, Kolkata

Name: Ms. Chandrima Gain

Supervisor: Dr. Abhik Saha
Assistant Professor**,** Wellcome Trust/DBT IA Fellow
School of Biotechnology, Presidency University, Kolkata

Title of the Thesis: Crosstalk between Proteasomal and Lysosomal Protein Degradation Pathway in EBV-Induced B-cell Lymphomas

PhD Registration No.: R-17RS18220100

Enrolment No.: PU/PHD/BIOS/2017/022

Place of Work: School of Biotechnology, Presidency University (2nd Campus)
Plot No. DG/02/02, Premises No. 14-0358, Action Area-ID
New Town (Near Biswa Bangla Convention Centre)
Kolkata-700156, West Bengal, India

Residential Address: 167/C, Dr. M.N. Saha Road. Dum Dum. Kolkata-700074. West Bengal

For Communication: 167/C, Dr. M.N. Saha Road. Dum Dum. Kolkata-700074. West Bengal

Email: chandrimagain31@gmail.com

Research scholar

(Full signature) Chandrima Gain

Forwarded Supervisor

(Full signature)

Crosstalk between Proteasomal and Lysosomal Protein Degradation Pathway in EBV-Induced B-cell Lymphomas

Introduction

The ubiquitin–proteasome system (UPS) and autophagy–lysosome pathways are the two main protein degradation pathways in eukaryotic cells [1][2]. Under the higher metabolic stress, cancer cells produce a massive amount of protein aggregates [3]. To maintain the normal protein homeostasis, these two protein clearance pathways execute an active participation and thereby avoiding cellular apoptosis [3][4]. The UPS and autophagy machineries are inter-connected by sharing several molecules either different regulators or substrates [5][6]. Moreover, in both these pathways the protein substrates are marked with ubiquitin molecules for targeted degradation[6]. The substrates tagged with K48-linked polyubiquitin chains are preferably degraded by the UPS, whereas K63-linked polyubiquitinated substrates are targeted by autophagy-lysosomal pathway [7][8][1].

EBV is the first human oncogenic virus discovered in 1964 [9]. It is associated with a number of human malignancies both of lymphoid and epithelial origin, predominantly in immune suppressed condition[10][11]. In vitro, EBV can readily alter quiescent B-lymphocytes into continuously proliferating lymphoblastoid cell lines (LCLs)[12]. These LCLs can be used as a surrogate system to study the EBV associated B-cell transformation and lymphoma development. During latency, EBV expresses a subset of genes including six nuclear antigens (EBNA-1, -2, -3A, -3B, -3C and -LP), 3 latent membrane proteins (LMP-1, -2A, -2B), 2 small non-coding RNAs (EBER-1 and 2) and BamHI-A rightward transcripts (BART) [10][13]. Along with EBNA2, EBNA3A, EBNALP and LMP1, EBNA3C plays a crucial role *in vitro* B-cell transformation and subsequent lymphoma development [14][15]. It manipulates multiple cellular pathways including cell-cycle/apoptosis and ubiquitin-targeted protein-degradation machineries. Previously it has been demonstrated that EBNA3C is ubiquitinated at its N-terminal domain and recruits SCF^{Skp2} E3 ligase to degrade a number of tumor suppressor proteins [16]. EBNA3C is also degraded *in vitro* by purified 20S proteasomes via interacting with the α-subunit of the 20S proteasome [17]. However, in proliferating B-lymphocytes, EBNA3C is extremely stable with a half life of more than 24h. Recently, our lab demonstrated that under growth limiting conditions EBNA3C elevates autophagy genes transcription as a survival strategy [18]. Additionally, K63-linked but not K48-lined poly-ubiquitination signals were significantly induced in EBNA3C expressing B-cells [18]. This signifies a potential connection between EBNA3C and autophagy regulated protein degradation pathway.

Recently, several proteasomal inhibitors have been approved for the treatment of hematologic malignancies [19][20]. In addition, studies have demonstrated a number of cell oncoproteins are degraded through autophagy-lysosomal pathway upon UPS inhibition [21][22]. Our study is aimed to investigate the underlying mechanism(s) regulating the degradation signal of EBNA3C as a therapeutic approach for several EBV associated B-cell lymphomas, particularly those are generated in an immunocompromised background. We also looked into the potential involvement of EBNA3C in manipulating the crosstalk among different protein degradation pathways.

Objectives

- Defining the underlying mechanism of Epstein-Barr virus oncoprotein EBNA3C's degradation
- Identification of EBNA3C's domain responsible for its degradation
- Exploring proteasomal and lysosomal inhibitors as potential therapeutic strategy against EBV associated B-cell lymphomas

Hypothesis

EBV encoded essential oncoprotein EBNA3C targets proteasomal and lysosomal protein degradation pathways in EBV-Induced B-cell Lymphomas.

Methodology

Drugs: MG132 (ab141003), bortezomib (ab142123) and Z-VAD (OMe)-FMK (ab120487) were obtained from Abcam (Cambridge, UK). Chloroquine diphosphate salt (C6628), Cyclohexamide (C7698), Leptomycin B (L2913), N-Acetyl-L-cysteine (A9165), Doxycycline hyclate (D9891), G418 sulfate (345810), 12-O-Tetradecanoylphorbol-13-acetate or TPA (P1585), sodium butyrate (B5887), Polybrene (TR-1003-G) and Puromycin dihydrochloride (P8833) were brought from Sigma-Aldrich Corp..

Plasmids: Myc-, flag-, GFP- and RFP-tagged EBNA3C constructs in pA3M, pA3F, pEGFP-C1 658 and pDsRED-Monomer-N1 vectors, respectively were previously described. Myc-tagged EBNA1 expressing construct in pA3M was described earlier. Myc- and flag-tagged EBNA3C 660 truncation constructs expressing EBNA3C residues 1-365, 366-620 and 621-992 were previously described. Myc-tagged EBNA3C N-terminal residues 1-365 expressing construct was used as a template for preparing three more EBNA3C truncations – residues 1-300, 1-250 and 50-300 in pA3M (pCDNA3.1-3X Myc) at EcoRI and NotI restriction sites. pA3M-EBNA3C construct was used as a template to clone GFP-tagged EBNA3C truncation constructs expressing residues 1-365 and 621-992 in pEGFP-C1 vector at EcoRI and SalI restriction sites. All the constructs were further verified by Sanger dideoxy based DNA sequencing (Eurofins Genomics India Pvt. Ltd., India). pEGFP-C1 and pDsRED-Monomer-N1 plasmids were obtained from Clontech Laboratories, Inc. mCherry-tagged p62 expressing plasmid was a kind gift from Edward M. Campbell (Loyola University Chicago, IL, USA). pBabePuro-GFP-LC3 construct was a kind gift from Jayanta Debnath (Addgene plasmid# 22405). pTripz-mCherry-Sh-Beclin1 construct (Clone ID: V2THS_23692) was obtained from GE Healthcare Dharmacon Inc. pGipz-Sh-Control and pGipz-Sh-EBNA3C were previously described.

Antibodies: Mouse monoclonal antibody against EBNA3C (A10) generated from hybridoma cells was previously described. Sheep polyclonal antibodies against EBNA3A (ab16126), EBNA3B (ab16127) and EBNA3C (ab16128) were bought from Abcam (Cambridge, UK). Rabbit polyclonal anti GFP (ab290), rabbit anti-Sheep IgG (H+L), rabbit polyclonal anti-Histone H3 (ab1791) and rabbit monoclonal anti-LMP1 (ab136633) antibodies were also obtained from Abcam. Mouse monoclonal antibodies directed against p62/SQSTM1 (Clone# 3/P62 lck ligand), Beclin1 (Clone# 20/Beclin), cleaved PARP (Clone# Asp214), total ubiquitin (Clone# 6C1.17) were purchased from BD Biosciences. Rabbit monoclonal antibodies directed against LC3A/B (Clone# D3U4C), K48-linkage specific polyubiquitin (D9D5) and K63-linkage specific polyubiquitin (D7A11) were purchased from Cell Signaling Technology Inc. Mouse monoclonal anti-flag (M2) and anti-cMyc (9E10) antibodies were purchased from Sigma-Aldrich Corp. Mouse monoclonal anti-MDM2 (SMP14), anti-p53 (DO-1) and anti-GAPDH (0411) antibodies were purchased from Santa Cruz Biotechnology. Rabbit polyclonal antibody against Lamin A/C (NB100-56649) was obtained from Novus Biologicals. DyLight 800/680 conjugated (for western blots) and Alexa Fluor 488/555 tagged (for confocal micoscopy) secondary antibodies anti-mouse, anti-rabbit, anti-sheep IgG (H+L) were purchased from Thermo Fisher Scientific Inc..

Cell lines and Cell culture: HEK293 cells were taken from Rupak Dutta (Indian Institute of Science Education and Research, Kolkata, India). HEK293T cells were purchased from GE Healthcare. Both HEK293 and HEK293T cells were maintained in Dulbecco's modified Eagle's medium (DMEM) (Gibco) supplemented with 10% fetal bovine serum (FBS) (Gibco/Invitrogen, Inc., USA), 1% Penicillin-Streptomycin Solution (Sigma-Aldrich Corp.). EBV-positive Burkitt's lymphoma (BL) cell line Namalwa was obtained from 700 National Centre for Cell Science, (NCCS, Pune, Govt. of India). EBV-negative BL lines – DG75, BJAB and BJAB stably expressing EBNA3A and EBV positive BL line Raji cells were obtained from Elliott Kieff (Harvard Medical School, USA). In vitro EBV transformed LCL clones (LCL#1 and LCL#89), EBV negative BL line BJAB, BJAB clones stably expressing either vector or EBNA3C cDNA (E3C#7) and lentivirus-mediated stable EBNA3C knockdown (LCL#Sh-E3C) or control (LCL#Sh-Con) lymphoblastoid cell lines (LCLs) were previously described. LCL#Sh-E3C and LCL#Sh-Con cells were freshly generated in LCL#1 as described below. BJAB-vector and BJAB-EBNA3C cells were maintained in complete RPMI media supplemented with 500 g/ml G418 (Sigma-Aldrich Corp.). LCL#sh-control media supplemented with 500 g/ml and LCL#sh-EBNA3C cells were maintained in complete RPMI media supplemented with 1μg/ml puromycin (Sigma-Aldrich Corp.). LCLs were maintained in RPMI 1640 (Gibco) supplemented with 10% FBS and 1% Penicillin-Streptomycin Solution. Unless otherwise stated all above-mentioned cells were cultured at 37ºC in a humidified environment supplemented with 5% CO_2.

Western blotting: Unless and otherwise stated, ~10 x 10^6 adherent or B-cells were harvested, washed with ice cold 1X PBS (Invitrogen), and subsequently lysed in 0.5ml ice cold RIPA buffer (Sigma-Aldrich Corp.) with protease inhibitor cocktail (Cell Signaling Technology Inc.). Protein concentrations were estimated by Bradford reagent (BIO-RAD). Samples were boiled in 2 X laemmli buffer (BIO-RAD), fractionated by SDS-PAGE and transferred to a 0.45 µm either nitrocellulose or low autofluorescence PVDF membranes (BIO-RAD). The membranes were then probed with specific antibodies followed by incubation with appropriate infrared-tagged/DyLight secondary antibodies and viewed on an Odyssey CLx Imaging System (LiCor Inc., USA). Image analysis and quantification measurements were performed using the Odyssey Infrared Imaging System application software (LiCor Inc.)**.**

Transfection: ~10 x 10^6 HEK293 cells were harvested, resuspended with 450 µL Opti-MEM medium (Invitrogen), mixed with appropriate plasmids in a 0.4-cm gap cuvette (BIO-RAD) and transfection was performed by electroporation using a Gene Pulser II electroporator (BIO-RAD) at 210 V and 975 µF for Western Blot analyses. Cells were harvested 36 h post transfection for western blot analyses, unless and otherwise stated. For confocal microscopy, cells were transfected with appropriate plasmids using Lipofectamine 3000 according to manufacturer's protocol (Thermo Fisher Scientific Inc.). 24 h post-transfection cells were subjected to live-cell confocal microscopy analyses.

Stability assay: ~5 x 10^6 EBV transformed B-lymphocytes (LCL#1) or EBNA3C stably expressing BJAB cells (BJAB-E3C#7) were treated with 100 µg/ml cyclohexamide (Sigma-Aldrich Corp.) alone (with DMSO control) or in the presence of 1 µM MG132 (Abcam Inc.) or 50 µM Chloroquine (Sigma-Aldrich Corp.) in normal growth medium for 24 h. Subsequently, lysates were prepared in 1 x RIPA buffer at indicated time periods and subjected to western blot analyses with appropriate antibodies. Band intensities were quantified by Odyssey imager (LiCor Inc.).

Confocal Microscopy: ~1 x 10^6 HEK293 cells grown at 70% confluency on 35 mm dish embedded with 12 mm glass viewing area (Nunc, Thermo Fisher Scientific Inc., Waltham, MA, USA) were transfected with appropriate plasmids using Lipofectamine 3000. 24 h post-transfection cells were either left untreated (DMSO control) or treated with 20 µM MG132 for another 4-6 h and subsequently subjected for live-cell confocal analyses. For live-cell imaging, Hoechst 3342 solution (Thermo Fisher Scientific Inc.) and LysoTracker Red DND-99 (Invitrogen, Thermo Fisher Scientific Inc., Waltham, MA, USA) were used to stain the nucleus and the acidic lysosomes, respectively. For LCLs, approximately 1 million cells either left untreated (DMSO control) or treated with 1 µM MG132 for 12 h were harvested in microcentrifuge tubes, washed with 1 X PBS, fixed and permeabilized with 4% paraformaldehyde (Sigma-Aldrich Corp.) and 0.1% Triton X-100 (Sigma-Aldrich Corp. St. Louis, MO, USA) followed by blocking with 5% BSA (BIO-RAD, Hercules, CA) at room temperature for 1 h. Cells were further incubated with appropriate primary antibodies for overnight at 40 C. Nucleus was counterstained with 4', 6',-diamidino-2-phenylindole (DAPI; BIO-RAD, Hercules, CA, USA) for 30' at room temperature. Alexa Fluor labeled secondary antibodies diluted in blocking buffer (1:2000) were incubated at room temperature for another 1 h. Cells were then washed for three times with 1 X PBS and mounted using an antifade mounting media (Sigma Aldrich Corp. St. Louis, MO, USA) in 8-well chamber slides (Thermo Fisher Scientific Inc.) for confocal microscopy. The images were obtained by a Leica DMi8 Confocal Laser Scanning Microscope and analyzed in the Leica Application Suite X (LAS X) software (Leica Microsystems GmbH). The intensities of stains were sometimes also analyzed by ImageJ software (https://imagej.nih.gov/ij/).

Real-Time quantitative PCR (qPCR): Total RNA was isolated from approximately 10 million LCLs (both LCL#1 and LCL#89) either left untreated (DMSO control) or treated with 1 µM MG132 for 12 h using TRIzol reagent according to the manufacturer's instructions (Invitrogen, Thermo Fisher Scientific Inc., Waltham, MA, USA), followed by cDNA preparation using iScript cDNA synthesis kit (BIO-RAD, Hercules, CA, USA) as per manufacturer's protocol. RNA and cDNA quality and quantity were checked using Synergy™ H1 Multimode Microplate Reader (BioTek Instruments, Inc., VT, USA). qPCR analysis was performed using iTaq Universal SYBR Green Supermix (BIO-RAD, Hercules, CA, USA) in CFX Connect™ Real-Time PCR detection System (BIO-RAD, Hercules, CA, USA) with the following thermal profile – 1 cycle: 950C for 10 min; 40 cycles: 950C for 15 sec followed by 600 C for 1 min; and finally the dissociation curve at – 95°C for 1 min, 55°C 30 min, and 95°C for 30 sec. Unless and otherwise stated, each sample was performed in duplicate and calculation was made using a $2^{-\Delta\Delta CT}$ method to quantify relative expression compared with housekeeping gene control. The real time PCR primers used in this study were designed from Primer-BLAST (https://www.ncbi.nlm.nih.gov/tools/primer-blast/) and listed in Table 1. Real-time PCR primers were obtained from Integrated DNA Technologies, Inc. (Coralville, IA, USA).

RNA-Sequencing and data analyses: ~1 µg of total RNA isolated from LCLs (both LCL#1 and LCL#89) either left untreated (DMSO control) or treated with 1 µM MG132 for 12 h was subjected to whole transcriptome enrichment through selective depletion of 99.9% of ribosomal RNA using RiboMinus™ Eukaryote Kit for RNA-Seq (Thermo Fisher Scientific Inc., Waltham, MA, USA) followed by library generation using Ion Total RNA-Seq Kit v2 (Thermo Fisher Scientific Inc., Waltham, MA, USA). Transcriptome analysis was performed in Ion S5TM XL System (Thermo Fisher Scientific Inc., Waltham, MA, USA). Reads generated from Ion S5 XL were subjected to further analysis with a minimum read length of 25 bp. The filtered in reads were aligned to human genome (hg19) using two-step alignment method. Reads were aligned using STAR and Bowtie software using default parameters. Both Alignment data were merged together using Picard. Reads aligning to reference genome were provided in bam format. Using the encode gene annotations for human genome (hg19), aligned reads were counted for each gene and were represented in standard format for all 4 samples. RNASeqAnalysis plugin (v5.2.0.5) was utilized to perform the analysis and produce gene counts for all the samples.

Using DESeq2 package from R, study for differential expression analysis was performed between sample conditions. It followed the negative binomial distribution for studying gene counts and tested each gene from samples for expression. Genes were selected based on p-value as <=0.05 and log2 Fold Change as 2 and above (up-regulated) and -2 and below (down-regulated). Differentially expressed gene sets were segregate together and subsequently uploaded on DAVID (Database for Annotation, Visualization and Integrated Discovery, version 6.8) webserver (https://david.ncifcrf.gov/) for further analyses. Features observed in different databases are clustered together for functional analysis. Gene Ontology (GO) was selected from the hits table for DAVID clustering. The clusters were represented through statistical analysis providing P-value and FDR (false discovery rate) in order to select functional significant clusters.

Induction of EBV lytic cycle from LCLs: ~10 x 10^6 LCLs (both LCL#1 and LCL#89) were induced to release virus in complete RPMI 1640 medium containing 20 ng/ml TPA (Sigma-Aldrich Corp.) and 3 mM sodium butyrate (Sigma-Aldrich Corp. St. Louis, MO, USA) for 24 h. To understand the role of proteasomal inhibition in EBV lytic cycle induction, LCLs were either left untreated (DMSO control) or treated with 1 µM MG132 for 24 h. Cells were then harvested and subjected for genomic DNA isolation using "Blood & Cell Culture DNA Mini Kit" (Qiagen, Hilden, Germany). Reactivation of LCLs was determined by real-time quantitative PCR (qPCR) analyses of EBV DNA targeting BamHI W genomic portion (Forward primer: 5'- CCCAACACTCCACCACACC-3'; reverse primer: 5'- TCTTAGGAGCTGTCCGAGGG-3'). As described above, the primers were synthesized from Integrated DNA technologies, Inc. (Iowa, USA).

Generation of Beclin 1 knockdown cells: ~10 x 10^6 HEK293 cells were transfected with pTripZ vector containing sh-Beclin1 sequence under doxycycline inducible promoter by electroporation. Sh-RNA expression was initiated using 1 µg/ml doxycycline (Sigma-Aldrich Corp.) and transfected cells were selected using 2 µg/ml of puromycin (Sigma-Aldrich Corp.) for 7 days. Without doxycycline treatment was served as control.

Colony formation assays: ~10 x 10^6 HEK293 stably transfected with pTripz-Sh-Beclin1 were either left untreated or treated with doxycycline to express the sh-RNA. 72 h post-treatment approximately 1 x 106 cells were further treated with DMSO control or 20 µM MG132 for 4 h in 100 mm petri-plates and selected in complete DMEM supplemented with 2µg/ml puromycin. Two weeks later, cells were fixed with 4% paraformaldehyde paraformaldehyde (Sigma-Aldrich Corp.) at room temperature for 0.5 h and stained with 0.1% crystal violet solution (Sigma Aldrich Corp. St. Louis, MO, USA) for 0.5 h. The plates were scanned using Odyssey CLx Imaging System (LiCor Inc.) and the relative colony number was measured by Image J software.

Co-immunoprecipitation assay: ~15 x 10^6 HEK293 cells transiently transfected with the indicated expression plasmids or 20 million LCLs were harvested, washed twice with ice cold 1 x PBS and subsequently lysed with 0.5 ml ice cold RIPA buffer, supplemented with protease inhibitors for 1 h on ice with brief vortexing every 5-10 minutes. The lysates were centrifuged at 13,000 rpm for 15 min at 4°C. 5 µl of each sample was taken out separately for measuring protein concentration using Bradford protein assay reagent (BIO-RAD). 5% of the lysates were boiled with 2 x laemmli buffer (BIO-RAD) and used as input. Lysates were precleared with control antibody plus 30 µL of 1:1 Protein-A/G magnetic beads (BIO-RAD, Hercules, CA, USA) for 1 h at 40 C. The protein of interest was captured by rotating the remaining lysate with 1 µg of specific antibody overnight at 40 C. Immuno-complexes were captured with 30 µL magnetic Protein-A/G beads, pelleted and washed 5 x with ice cold RIPA buffer. Input lysates and IP complexes were

boiled in 2 x laemmli buffe, fractionated by SDS-PAGE and transferred to either 0.45 µm nitrocellulose or PVDF membrane for western blot analyses as described above on an Odyssey imager.

***In vivo* ubiquitination assay:** ~15 x 106 HEK293 cells were transfected with flag-tagged EBNA3C constructs expressing either full-length protein (residues 1-992) or various domains N-terminal (residues 1-365), middle part (residues 366-620) and the C-terminal (residues 621-992). 36h post-transfection cells were further incubated with 20 µM MG132 for an additional 4 h before harvesting. After washing with 1 x PBS, cells were lysed in 100 µl RIPA buffer containing 1% SDS, boiled for 10 minutes to disrupt any protein-protein interaction. Each lysate was subsequently mixed with 900 µl of RIPA buffer without SDS to dilute the SDS concentration to 0.1%, incubated at 40 C on rotator for 1 h and centrifuged at 13,000 rpm for 15 min at 4°C. The supernatant was collected to a new tube and precleared with control antibody plus 30 µL of 1:1 Protein-A/G magnetic beads for 1 h at 40 C. Flag-tagged EBNA3C proteins were immunoprecipitated with 2 µg M2 antibody for overnight at 40 C, captured by 1:1 Protein-A/G magnetic beads, washed 5 x with ice cold RIPA buffer, and boiled in 2 x laemmli buffer. The extent of ubiquitination of flag-tagged proteins was determined by SDS PAGE followed by western blot analysis using indicated antibodies against total ubiquitin or specific to K48- or K63-linked polyubiquitination.

Subcellular fractionation assay: ~10 x 10^6 HEK293 cells transiently transfected for 36 h with the indicated EBNA3C expression plasmids were either left untreated (DMSO control) or treated with 20 µM MG132. Cells were harvested and subsequently subjected to subcellular fractionation as per manufacturer's protocol (BIO-RAD, Hercules, CA, USA). Nuclear and cytoplasmic protein fractions were measured by Bradford protein assay (BIO-RAD, Hercules, CA) and ~50 µg of total protein was resolved by SDS-PAGE. The efficiency of nuclear and cytoplasmic fractionation was confirmed by western blot analyses against nuclear protein Histone or lamin A/C and cytoplasmic protein GAPDH, respectively.

Soft agar assay: Soft agar assays were performed for LCLs (both LCL#1 and LCL#89). 0.75% agar (Sigma-Aldrich Corp. St. Louis, MO, USA) in 1 ml complete RPMI 1640 medium was poured into each well of 6-well plates (Corning Inc., NY, USA) and set aside to solidify. Next, 1 × 105 LCLs either left untreated (DMSO control) or treated with MG132 (1-5 µM) or bortezomib (0.5-1 µM) for 24 h, were harvested, mixed with 1 ml complete RPMI 1640 medium supplemented with 0.36% agar and poured on the top of the hard agar (1%) layer. Two weeks later, colonies were stained with 0.1% crystal violet for 30 minutes and scanned using Odyssey CLx Imaging System (LiCor Inc., Lincoln, NE, USA) and the relative colony number was measured by Image J software. Prior to staining, each well 894 was also photographed (bright-field) using a ZOE™ Fluorescent Cell Imager (BIO-RAD, Hercules, CA, 895 USA).

Cell viability assay: ~0.5 × 105 cells plated into each well of the six-well plates (Corning Inc.) were treated with either MG132 or bortezomib at increasing concentrations (0-10 µM) for the indicated time points at 370 C in a humidified CO2 chamber. Viable cells from each well were measured by Trypan blue exclusion method using an automated cell counter (BIO-RAD, Hercules, CA). Experiments were performed in duplicate and were independently repeated two times.

Statistical analysis: All the data represented are as the mean values with standard deviation 914 (SD). Statistical significance of differences in the mean values was analyzed using the Student's t-test 915 two tail distribution and equal variances between two samples. P-value below 0.05 was considered 916 as significant (*P < 0.05; **P < 0.01; ***P < 0.001; NS, not significant).

Results

❖ Objective I: Defining the underlying mechanism of Epstein-Barr virus oncoprotein EBNA3C's degradation

Studies have shown that proteasomal inhibition results in degradation of many important cellular oncoproteins involving autophagy-lysosomal pathway. Which triggered us most was that the expression of oncogenic mutant p53 is significantly lowered in cancer cells upon proteasomal inhibition [22]. The well studied interactive pattern of EBV

essential antigen EBNA3C with the protein degradation machineries led us to explore the mechanism that maintains the extraordinary stability of this viral oncoprotein in growing EBV transformed B-lymphocytes.

Proteasomal inhibition facilitates degradation of EBV essential nuclear antigen EBNA3C: To determine the half-life of EBNA3C protein affected by UPS and autophagy lysosomal pathway, EBV transformed lymphoblastoid cell line (LCL#1) was treated with protein synthesis inhibitor, cyclohexamide (CHX) for 24 h in the absence (DMSO control) or in the presence of proteasome (MG132, 1 µM) or autophagy-lysosomal (Chloroquine, CQ, 50 µM) inhibitors (Fig. 1A). Unexpectedly, the western blot analysis demonstrated that instead of increasing EBNA3C stability, MG132 treatment decreased EBNA3C stability (half-life: ~12 h) in comparison to the DMSO treated cells (half-life: >24 h), whereas CQ treatment results in enhancement of the overall EBNA3C protein stability (Fig. 1A). To rule out the possible effect of MG132 in transcriptional regulation, a similar experiment was performed using EBNA3C stably expressing BJAB cells (BJAB-E3C#7) (Fig. 1B). As before, a similar result was obtained (Fig. 1B), confirming that MG132 mediated EBNA3C's degradation is being manipulated at the protein level. However, no sign of EBNA3C's degradation was detected upon autophagy induction in absence of growth promoting signals (Earle's Balanced Salt Solution, EBSS) for 9 h (Fig. 1C). In contrast, a dose dependent degradation pattern of EBNA3C was obtained with increasing concentrations of MG132 (0-40 µM) treated for 4 h (Fig. 1D). Overall, these data indicate that proteasomal inhibition by MG132 enhances EBNA3C's degradation and autophagy-lysosomal pathway might play an important role in regulating EBNA3C stability.

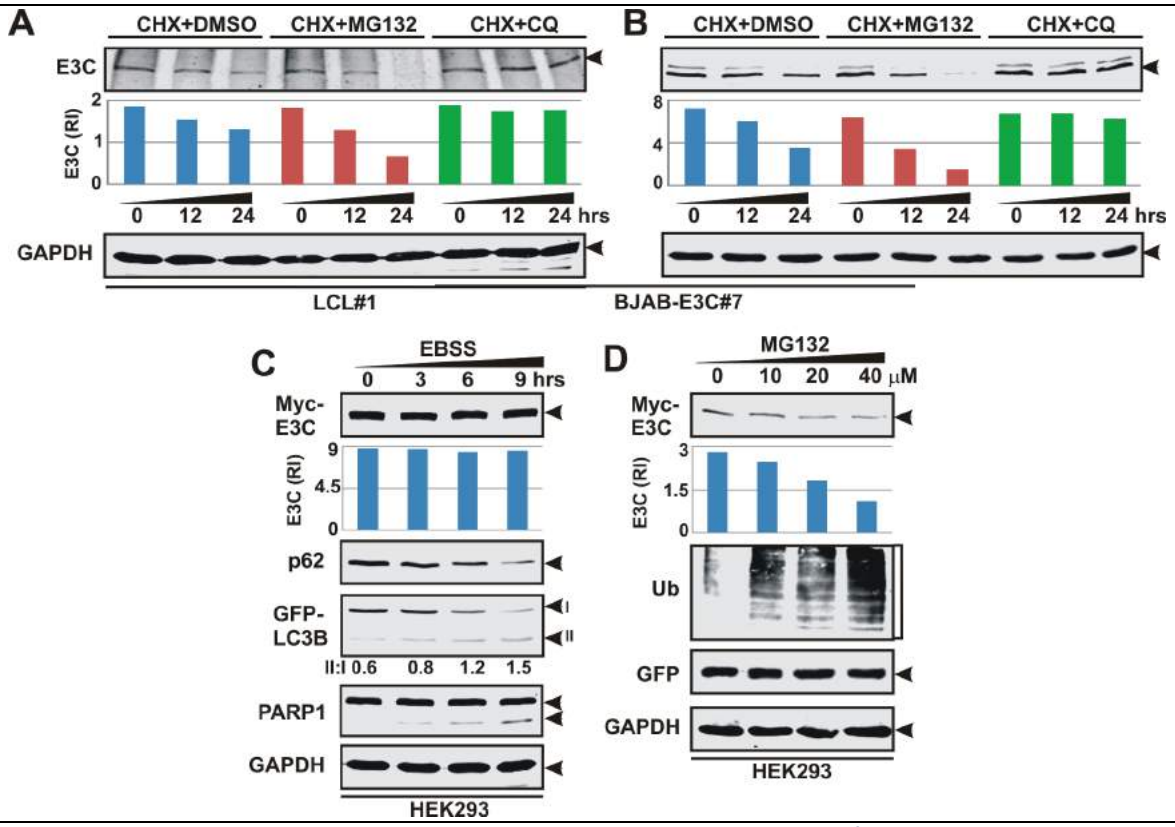

Fig. 1. Proteasome inhibition leads to degradation of EBV essential antigen EBNA3C. (A) ~10 x 10^6 LCL#1 and (B) BJAB-E3C#7 cells were treated with protein synthesis inhibitor, cyclohexamide (CHX) for 24 h in the absence (DMSO control) or in the presence of 1 µM proteasome inhibitor MG132 or 50 µM autophagy-lysosomal inhibitor Chloroquine (CQ). HEK293 cells transfected with myc-tagged EBNA3C were incubated with (C) EBSS to induce autophagy for 9 h or (D) increasing concentrations of MG132 (0-40 µM) for 4 h. In each experiment, cells were harvested after drug treatment and subjected for western blot analysis with indicated antibodies. GAPDH was used as loading control. The relative intensities (RI) of protein bands shown as bar diagrams were quantified using the software provided by Odyssey CLx Imaging System. Representative gel pictures are of at least two independent experiments.

Proteasomal inhibition leads to degradation of latent oncoproteins - EBNA3A and EBNA3C, but not EBNA3B: All three EBNA3 family proteins share ~30% sequence homology near the N-terminal region and are extremely stable in growing B-lymphocytes [23]. To determine whether EBNA3A and/or EBNA3B proteins were also similarly regulated in LCLs when proteasome was inhibited, LCLs were treated with MG132 or DMSO and subjected to western blot and cofocal analyses (Fig. 2A-B). MG132 treatment resulted in a prominent decrease in expressions of both EBNA3A and

EBNA3C viral oncoproteins, whereas unexpectedly no sign of degradation was observed for the third member of EBNA3 family proteins - EBNA3B, a non-essential viral latent antigen during B-cell transformation (Fig. 2A-B). Using a similar experimental set-up, we also demonstrated that alike MG132, bortezomib, an FDA-approved proteasomal inhibitor, induced an effective degradation phenomenon of both EBNA3A and EBNA3C proteins (data not shown).

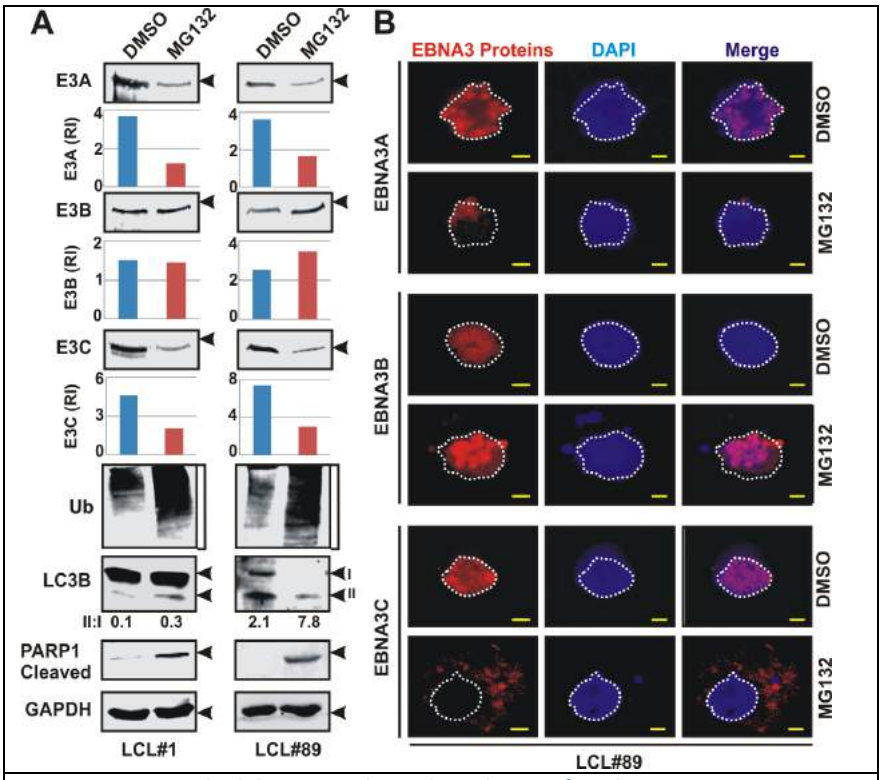

Fig. 2: Proteasomal inhibition results in degradation of viral oncoproteins - EBNA3A and EBNA3C, but not EBNA3B in LCLs. LCLs treated with DMSO or MG132 and subjected to (A) WB and (B) Confocal analyses with the indicated antibodies.

Proteasomal inhibition transcriptionally activates autophagy pathway and viral genes: To investigate the global effect of proteasomal inhibition at transcriptional level, RNA-Seq experiment was performed. Analyzing the transcript levels of genes deregulated in LCLs upon MG132 treatment, it was found out that genes involved in autophagy initiation (p62/*SQSTM1*, *MAP1LC3B*, *GABARAPL1*, *CTSD*, *UBC*), or protein folding and regulation of cellular response to various cellular insults such as unfolded protein response (UPR) and chaperone mediated autophagy (*HSPH1*, *HSP90AA1*, *HSPA2*, *HSPB1*, *DNAJB1*, *DNAJB4*, *SERPINH1*, *HSPA8*, *HSP90AA4P*, *HSP90AB3P*, *BAG3*) was significantly increased in presence of MG132, as compared to the control LCLs (Fig. 3A-C). However, there was a drastic reduction of transcripst levels of genes associated with DNA replication and nucleosome assembly (Fig. 3A-B). The RNA-Seq data were further validated by qRT-PCR assays in both LCLs (Fig. 3B-C)

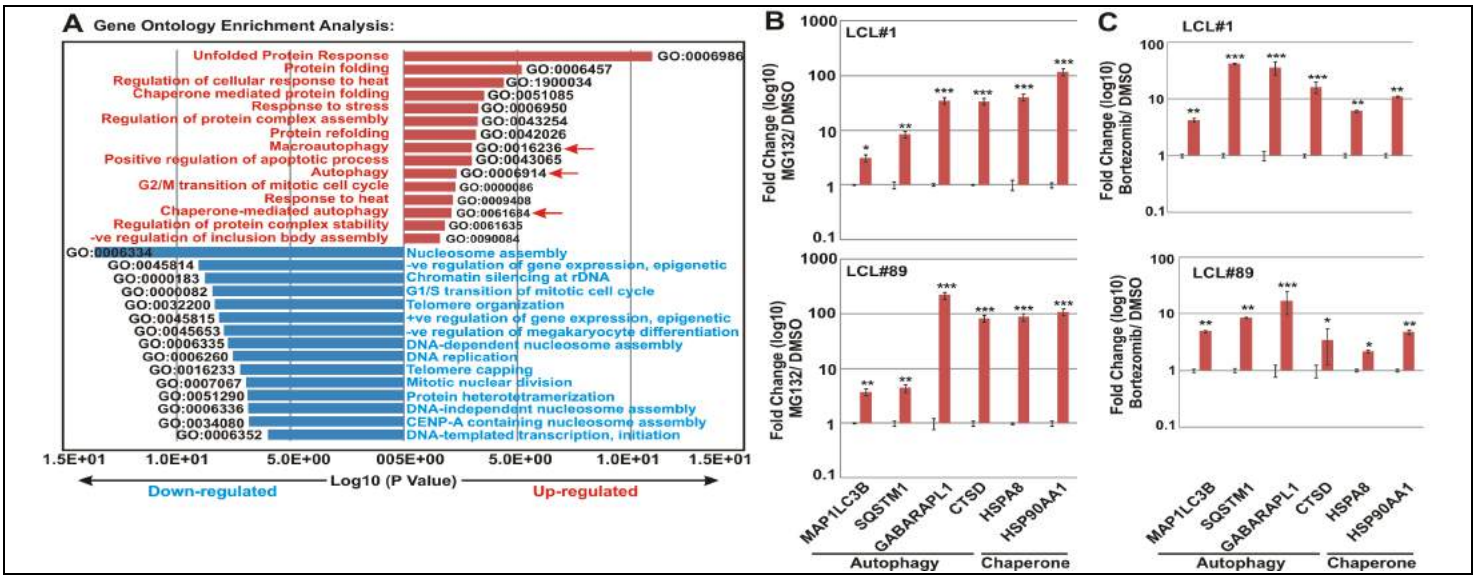

Fig. 3: Proteasomal inhibition leads to transcriptional activation of autophagy genes. (A) The cDNA samples prepared from LCLs treated with DMSO or MG132 were subjected to whole transcriptome analyses (RNA-Seq). Differentially expressed gene sets were uploaded on DAVID v6.8 webserver for functional analysis. Gene Ontology (GO) was selected from the hits table for DAVID clustering. The bar diagrams (upregulated: red; downregulated: blue) represent top 15 most significantly affected pathways. qPCR analyses of the selected cellular genes in LCLs treated with DMSO or proteasome inhibitors – (B) MG132, (C) bortezomib.

Autophagy stimulated by proteasomal inhibition is required for the degradation of EBNA3C: Autophagy activation upon MG132-treatment, prompted us to further investigate that whether autophagy-lysosomal pathway is

responsible for EBNA3C-degradation when proteasome is inhibited. Aautophagy pathway was either blocked by chemical inhibitors - bafilomycin or chloroquine (CQ) treatment or by Beclin 1 knockdown (Fig. 4A-D). Overall the results suggest that the increased degradation of EBNA3C complementing with reduced oncogenic potential observed with MG132 treatment was mediated at least in part by the autophagy-lysosomal pathway (Fig. 4).

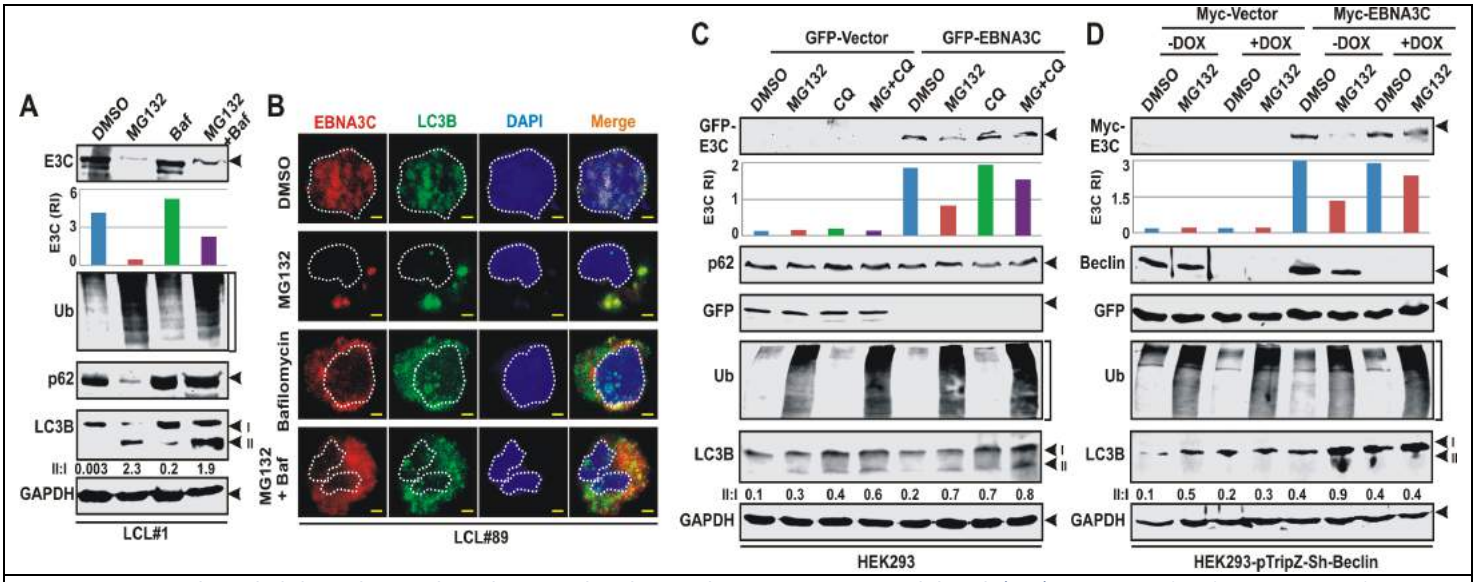

Fig. 4. EBNA3C is degraded through autophagy-lysosomal pathway when proteasome is inhibited. (A-B) LCLs treated with DMSO control, MG132, bafilomycin (Baf) or MG132 plus Baf for 24 h were subjected to (A) WB analysis or (B) immunostaining with the indicated antibodies. (C) HEK293 cells or (D) HEK293 cells stably expressing sh-Beclin 1 under doxycycline (Dox) inducible promoter transiently transfected with the indicated plasmids were further treated with different drugs as indicated and subjected to WB analyses for the indicated antibodies.

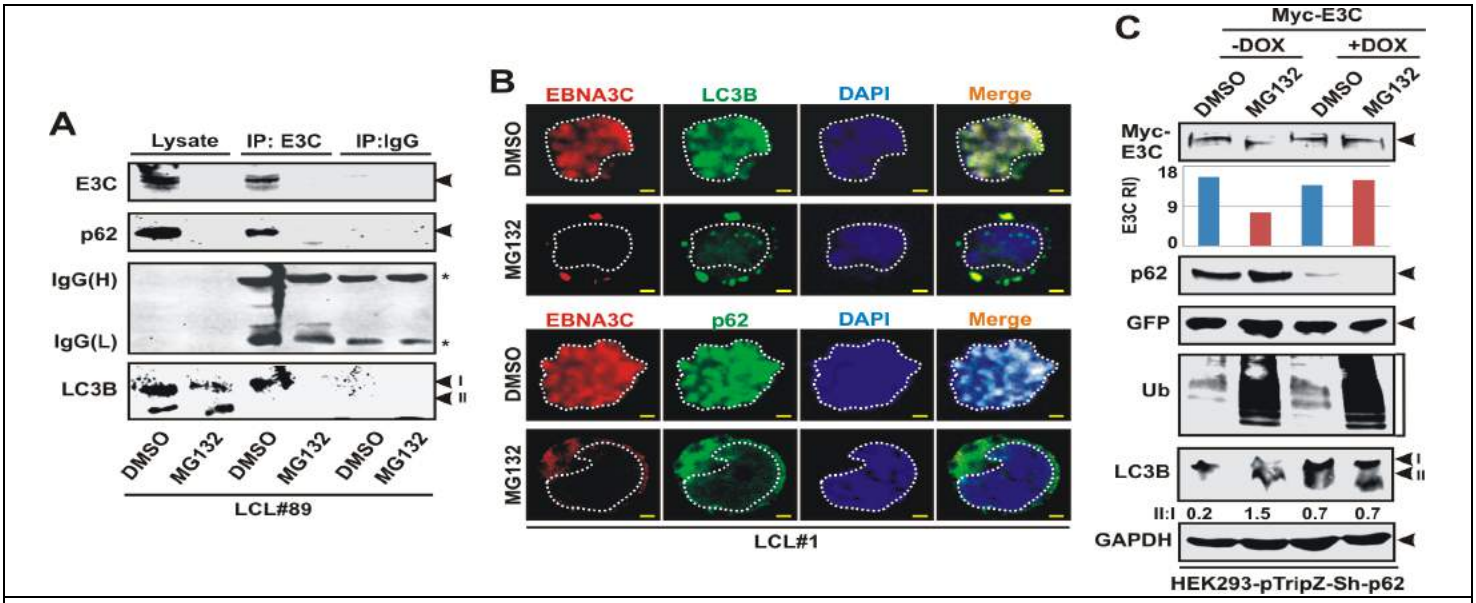

Fig. 5. EBNA3C is degraded through autophagy-lysosomal pathway when proteasome is inhibited. (A-B) LCLs treated with DMSO control, MG132, bafilomycin (Baf) or MG132 plus Baf for 24 h were subjected to (A) WB analysis or (B) immunostaining with the indicated antibodies. (C) HEK293 cells or (D) HEK293 cells stably expressing sh-Beclin 1 under doxycycline (Dox) inducible promoter transiently transfected with the indicated plasmids were further treated with different drugs as indicated and subjected to WB analyses for the indicated antibodies.

EBNA3C interacts and colocalizes with p62-LC3B complex in the cytoplasmic fraction when proteasome is compromised: To determine whether EBNA3C can participate within the p62-LC3B complex, we performed immunoprecipitation experiments in LCLs with or without MG132 treatment (Fig. 5A). p62-LC3B complex was evidently precipitated with EBNA3C pull-down in DMSO treated LCLs, however, due to severe degradation of EBNA3C as well as p62 (increase of autophagy flux) in MG132 treated LCLs resulted in lack of effective protein concentrations and accordingly no complex formation was detected when pull-down with anti-EBNA3C antibody as similar to mouse IgG control (Fig. 5A). Immunofluorescence studies demonstrated that MG132 treatment caused a drastic reduction of

EBNA3C puncta formation in the nucleus compartments and increase in colocalization with both LC3B and p62 independently in the cytoplasmic fraction (Fig. 5B). Participation of EBNA3C within p62-LC3B complex prompted us to further investigate whether p62 acts as an adaptor for EBNA3C degradation through autophagy-lysosomal pathway. To this end, HEK293 cells were stably knockdown for p62 by transfecting a lentiviral sh-p62 expressing construct under doxycycline inducible promoter (Fig. 5C). EBNA3C degradation induced by MG132 treatment was partially rescued when p62 expression was depleted in the presence of doxycycline treatment (Fig. 5C). Overall, the results indicated that p62-LC3B binds to EBNA3C in physiological conditions, mediating its degradation via the autophagy-lysosomal pathway when proteasome is inhibited.

EBNA3C is predominantly K63-linked polyubiquitinated when proteasome is inhibited: Studies have shown that proteins linked with K48 ubiquitin are degraded through proteasomal pathway, whereas K63-tagged substrates are targeted via autophagy [24][25]. Previous data has suggested that EBNA3C can be polyubiquitinated at the N-terminal domain [16]. Moreover, the ubiquitin associated UBA domain of p62 bind to both K48- and K63-linked polyubiquitin chains regulating the fate of autophagic protein turnover [25][26]. These intrigued us to further look into the pattern of polyubiquitin chains linked with EBNA3C upon MG132 treatment.

Immunofluorescence assays using specific antibodies against in LCLs either left untreated (DMSO control) or treated with MG132, illustrated that EBNA3C is mostly colocalized with ubiquitin irrespective its ubiquitination pattern and it is present within the nuclear compartments for DMSO control. However, in presence of MG132, there was a change in colocalization pattern from nuclear to predominantly cyctoplasmic (Fig. 6A). Western blot analyses using a similar experimental set up confirmed that MG132 treatment significantly enhanced both total ubiquitination and K48-linked polyubiquitination levels destined for proteasomal degradation (Fig. 6B). On the other hand, both EBNA3C and K63-linked polyubiquitination level was notably lowered in presence of MG132, indicating that K63-linked polyubiquitinated substrates (including EBNA3C) are recycled in autophagy-lysosomal pathway, upon proteasomal inhibition (Fig. 6B). Full blot analyses of EBNA3C (~120 kDa) western blots using two different antibodies (mouse monoclonal followed by a sheep polyclonal) demonstrated the degradation/proteolytic cleavage pattern, identifying two predominant bands – one at ~75 kDa and another at ~45 kDa (Fig. 6B). Validation of EBNA3C polyubiquitination pattern was done by conducting *in vivo* ubiquitination experiments in the absence and presence of MG132 under denaturing conditions allowing only covalent modifications (Fig. 6C). The results confirmed that MG132 treatment specifically enhanced K63- but not K48-linked polyubiquitination of EBNA3C (Fig. 6C).

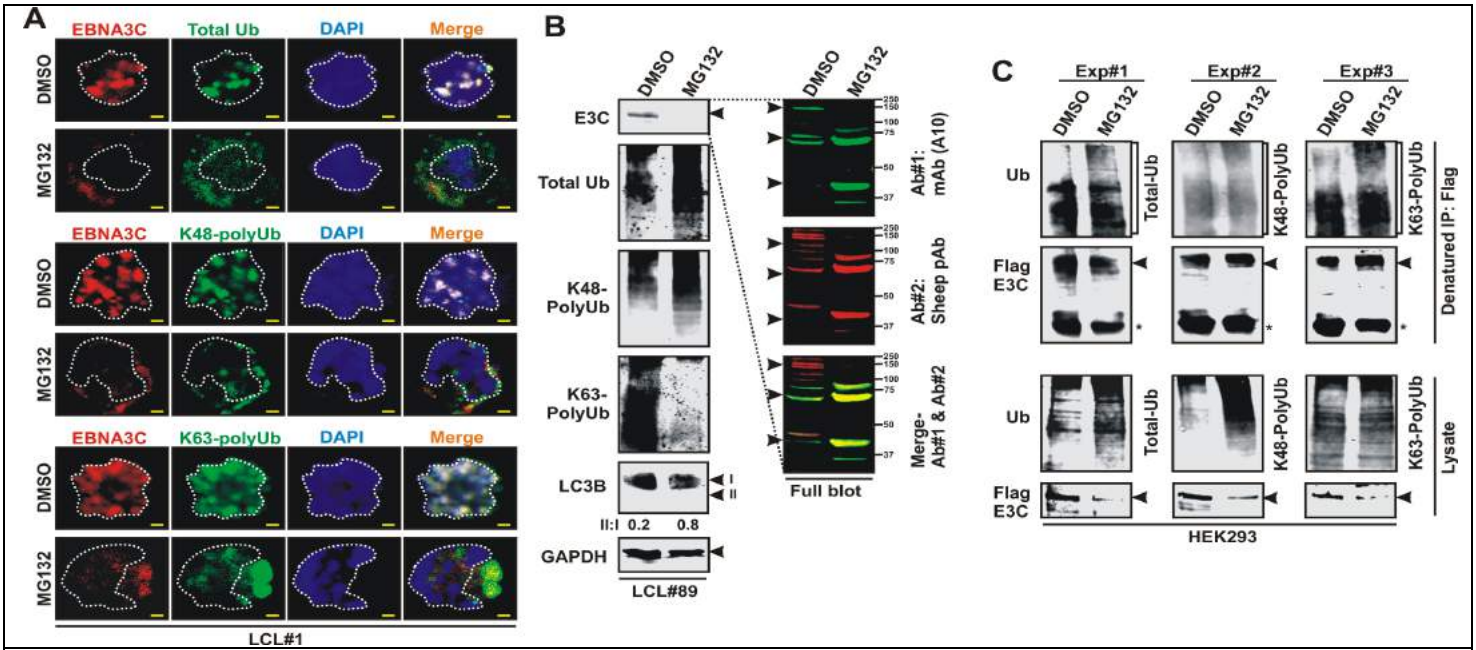

Fig. 6. Upon proteasomal inhibition EBNA3C is K63-linked polyubiquitinated. LCLs were treated with DMSO or 1 µM MG132 for 12 h and subjected for (A) immunostaining with EBNA3C, total ubiquitin (Ub), K48- and K63-linked polyubiqitination specific antibodies; (B) western blot analyses with indicated antibodies. (A) Nuclei were counterstained with DAPI before mounting the cells for confocal analyses. (C-D) HEK293 cells transiently transfected with flag-tagged EBNA3C expression vector, either left untreated (DMSO control) or treated with 20 µM MG132 for 4h were subjected for (C) western blot analyses or (D) immunoprecipitation (IP) under denatured conditions using anti-flag antibody followed by western blot analyses using indicated antibodies.

❖ Objective II: Identification of EBNA3C's domain responsible for its degradation

N-terminal domain of EBNA3C is important for autophagy mediated degradation in response to proteasomal inhibition: Earlier demonstration of polyubiquitination at the N-terminal domain (residues 1-159) of EBNA3C led us to further explore the domain(s) responsible for autophagy mediated degradation in response to proteasomal inhibition. To this end, HEK293 cells were transiently transfected with flag-tagged EBNA3C constructs expressing EBNA3C residues 1-365 (N-terminal), residues 366-620 (middle part) and residues 621-992 (C-terminal). As described earlier, 36h post-transfected cells were treated with DMSO and MG132 (20 µM) or CQ (50 µM) for another 4 h (Fig. 7A). The results demonstrated that only MG132 treatment caused significant reduction in expression of EBNA3C N-terminal domain as compared to DMSO or CQ treated cells (Fig. 7A). However, there was little or no change of ectopic expression levels of other two domains ranging from residue 366 to residue 992 in the absence or presence of both proteasomal and autophagy inhibitors (Fig. 6A). LC3II conversion confirmed autophagy activation, while enhanced polyubiquitination validated effective proteasomal inhibition upon MG132 treatment (Fig. 7A). *In vivo* ubiquitination experiments also validated polyubiquitination of EBNA3C at the N-terminal domain (residues 1-365) both in physiological conditions (DMSO control) and when proteasome is inhibited by MG132 (Fig. 7C).

A potential PEST (proline, glutamic acid, serine and threonine) sequence 'HDQDPGPGPPSSGASER' was identified near the N-terminal domain (residues 28-44) (Fig. 7D). In order to determine whether this identified PEST sequence is responsible for autophagy dependent degradation in response to proteasomal inhibition, three more flag-tagged EBNA3C truncated constructs were generated expressing residues 50-300 (lacking PEST motif), residues 1-300 and residues 1-250. HEK293 cells transiently transfected with these constructs along with EBNA3C residues 1-365 expressing plasmid were subjected to western blot analyses after treatment with either DMSO control or MG132 (Fig. 7B). While MG132 treatment caused obvious stabilization of residues 50-300, significant reduction of protein expression was observed when first 50 residues were included in all three EBNA3C truncations (Fig. 7B). Taken together, the results indicated that EBNA3C N-terminal first 50 residues containing PEST sequence might be responsible for autophagy-lysosomal mediated degradation when proteasome is inhibited.

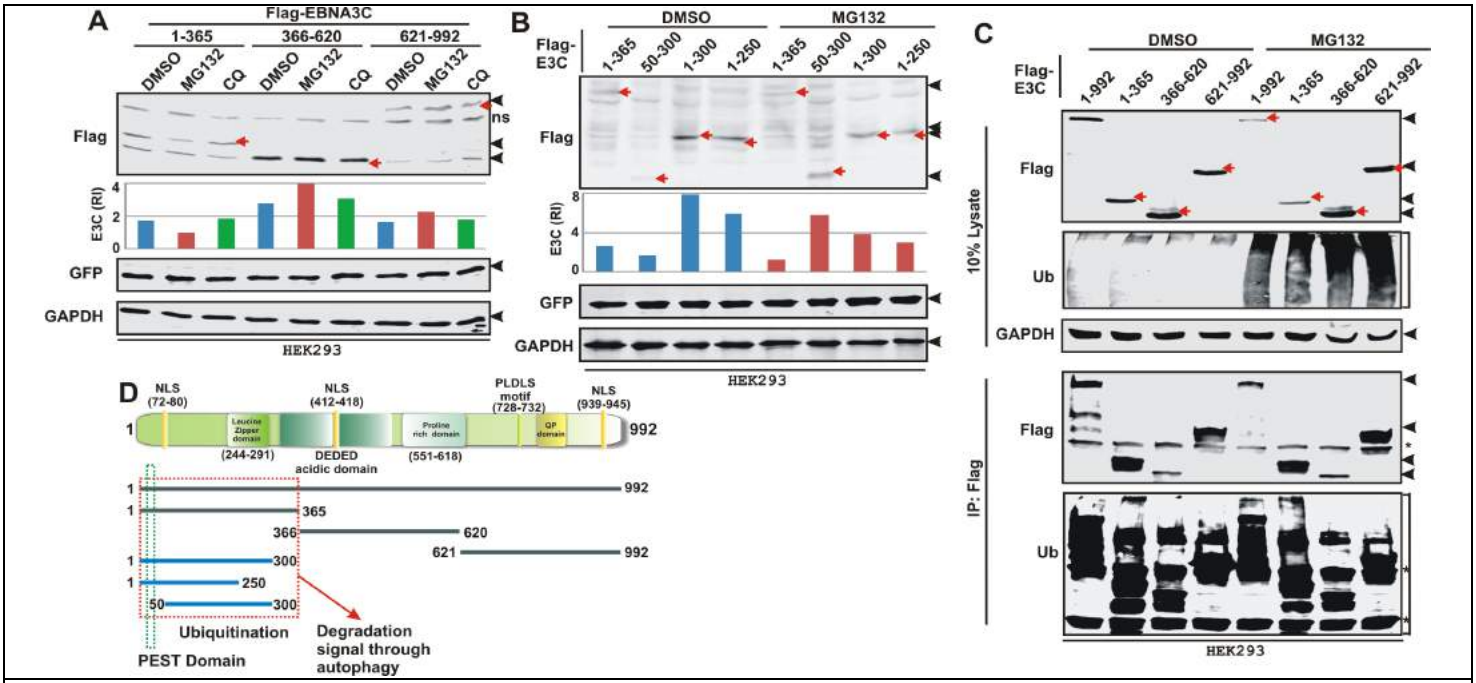

Fig. 7. N-terminal domain of EBNA3C is important for autophagy mediated degradation in response to proteasomal inhibition. (A-B) HEK293 cells transiently transfected with plasmids expressing flag-EBNA3C truncations, were treated with DMSO or MG132 and subjected for WB analyses with the indicated antibodies. (C) Using a similar experimental set up, HEK293 cells transiently transfected with full-length (residues 1-992) and different domains of flag-tagged EBNA3C expression constructs were subjected to immunoprecipitation (IP) with anti-flag antibody followed by WB analyses with the indicated antibodies after stripping and reprobing the same membrane. (D) The schematic illustrates known structural motifs and different domains of EBNA3C that are used to determine residues important for autophagy mediated degradation upon proteasomal inhibition.

EBNA3C N-terminal domain is degraded in the both nuclear and cytoplsamic fractions upon proteasomal inhibition: In order to continue exploring the mechanisms involved in EBNA3C degradation, we identified two potential

NES-sequences near the N- and C-terminal regions for EBNA3C (Fig. 8A). However, no predicted NES-sequences were found for both EBNA3A and EBNA3B proteins. Subcellular fractionation assay using HEK293 cells transiently transfected with myc-EBNA3C demonstrated that EBNA3C was indeed fractionated in both nuclear and cytoplasmic sections and upon MG132 treatment EBNA3C was specifically found to be degraded in the cytoplasmic fraction (Fig. 8B). Live-cell confocal-microscopy analysis in HEK293 cells transiently transfected with GFP-tagged EBNA3C also demonstrated that MG132 treatment resulted in co-localization of EBNA3C with the lysosomal fraction in the cytoplasm (Fig. 8C). Using leptomycin-B, a nuclear export inhibitor by targeting exportin 1, our result also suggests that EBNA3C degradation might occur in both nuclear and cytoplasmic compartments (Fig. 8D-E). Using various EBNA3C-truncations we demonstrated that MG132 treatment led to degradation of the N-terminal domain in both nuclear and cytoplasmic fractions, whereas the C-terminal domain was somewhat stabilized in both fractions (Fig. 8F-K). In contrast, the middle part appears to be unaffected in the nuclear fraction (Fig. 8G and H). Although leptomycin B treatment did not have any influence on degradation pattern of EBNA3C domains, it significantly affected cytoplasmic translocation of the C-terminal domain as similar to the full-length protein induced upon proteasomal inhibition (Fig. 9A-C). Taken together, the results suggest that nuclear export signal residing at both N- terminal and C-terminal domains play a crucial role for EBNA3C degradation in the cytoplasm through autophagy mechanism when proteasome is inhibited or overloaded due to accumulation of mis-/un-folded proteins.

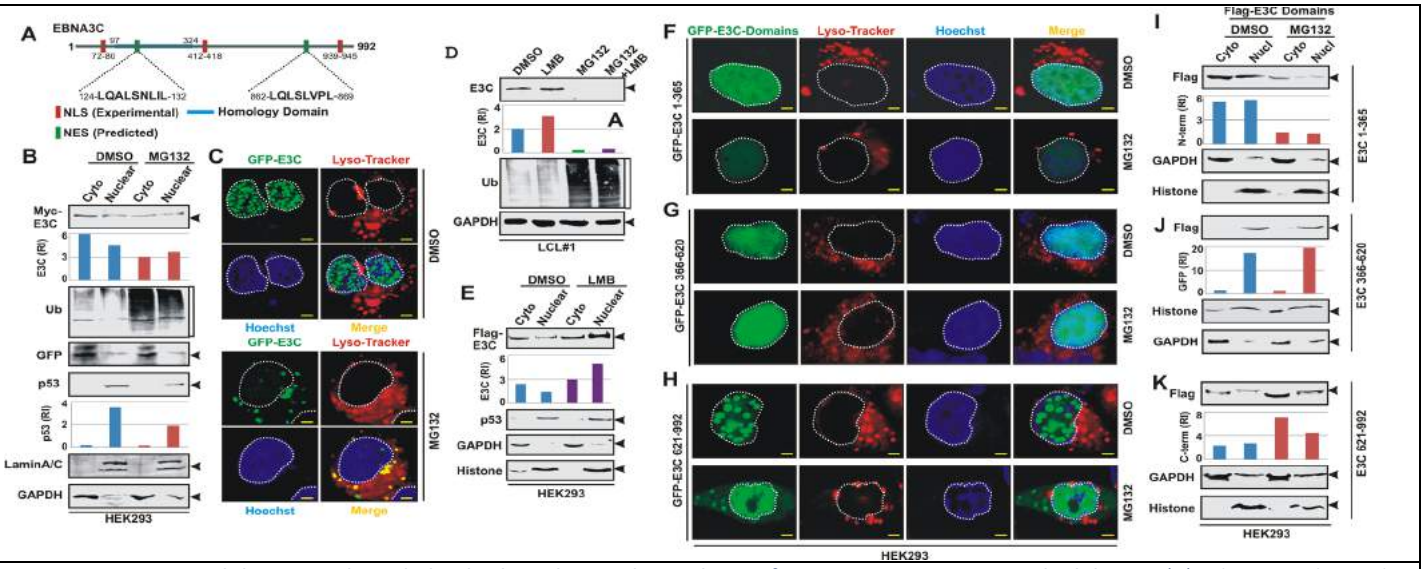

Fig. 8. EBNA3C N-terminal domain is degraded in both nuclear and cytoplsamic fractions upon proteasomal inhibition. (A) Schematic shows the predicted nuclear export signal (NES) sequences of EBNA3C. (B-C) HEK293 cells transfected with the indicated expression plasmids were further treated with DMSO or MG132 and subjected to (B) subcellular fractionation followed by western blot analyses and (C) live cell confocal analyses. (D) LCLs treated with different drugs were subjected to WB analysis. (E) HEK293 cells transfected with Flag-EBNA3C were treated with DMSO or Leptomycin B (LMB) and subjected to WB analyses. HEK293 cells transiently transfected with plasmids expressing (F-H) GFP-tagged or (I-K) flag-tagged different EBNA3C domains in a similar experimental set up were subjected to (F-H) live cell confocal microscopy or (I-K) subcellular fractionation followed by WB analyses.

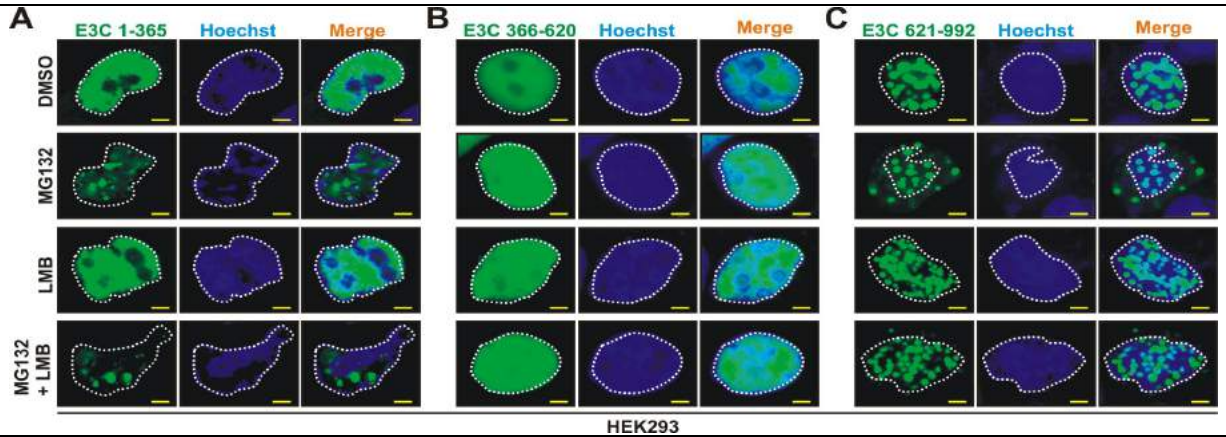

Fig. 9: EBNA3C fractionation in the absence and presence of leptomycin B. HEK293 cells transfected with GFP-tagged different EBNA3C constructs were treated with different drugs and subjected to live cell confocal microscopy.

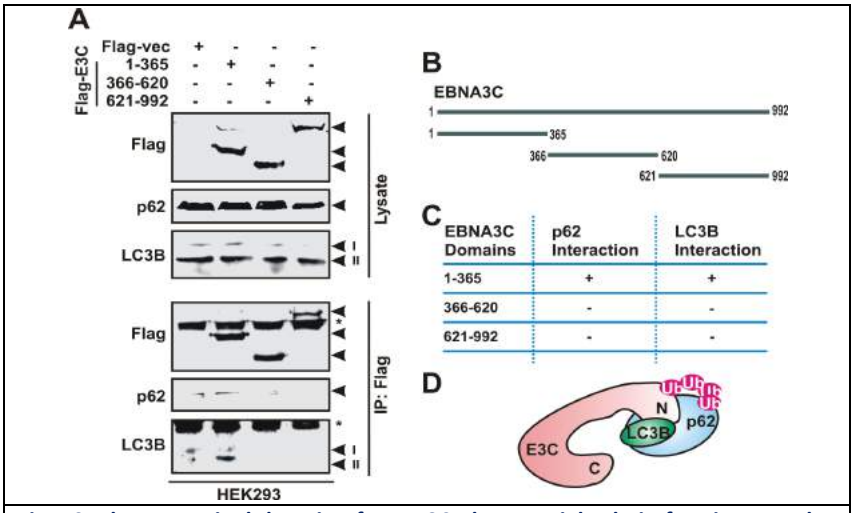

Fig. 10. The N-terminal domain of EBNA3C plays crucial role in forming complex with p62 and LC3B. (A) HEK293 was cells transiently transfected with different flag-tagged EBNA3C truncations and subjected to co-immunoprecipitation with anti-flag antibody followed by western blot analyses with the indicated antibodies. * indicates IgG bands. (B) Pictorial representation of EBNA3C truncations used in the co-immunoprecipitation experiment. (C-D) Summary and cartoon representation of the interaction study of different EBNA3C domains with p62 and LC3B.

The N-terminal domain of EBNA3C plays crucial role in forming complex with p62 and LC3B: Since the autophagy mediated proteolytic signal is located at the N-terminal region of EBNA3C (residues 1–50), next we wanted to determine whether the N-terminal domain forms a complex with autophagy components – including both p62 and LC3B. To this end, HEK293 cells transiently transfected with either vector control or flag-tagged EBNA3C expressing constructs including the N-terminal (residues 1-365), middle part (residues 366-620) and C-terminal (residues 621-992) domains were subsequently subjected for co-immunoprecipitation experiments with ant-flag-antibody (Fig. 10A). The results demonstrated that the only N-terminal domain bound to both p62 and LC3B (Fig. 10A-D), which likely initiates EBNA3C degradation via autophagy-lysosomal pathway.

❖ Objective III: Exploring proteasomal and lysosomal inhibitors as potential therapeutic strategy against EBV associated B-cell lymphomas

Several potential therapeutic strategies have been described with transcriptional activation of EBV lytic-genes using multiple chemotherapeutic agents such as HDAC inhibitor (sodium butyrate; NaBu) in combination with a protein kinase C activator (12-O-tetradecanoylphorbol-13-acetate; TPA) [27][28][29]. Bortezomib treatment can also enhance EBV lytic-gene transcription through UPR gene C/EBPβ [30]. However, the effect of proteasomal inhibition on other viral genes – both lytic and latent was not explored. To evaluate the effect of proteasomal inhibition at the transcriptional level of viral genes qRT–PCR assays were performed in LCLs either left untreated or treated with proteasome inhibitors - MG132 and bortezomib (Fig. 11A, C, E, G). The results demonstrated that proteasomal inhibition enhanced both lytic and latent genes transcription including EBNA3A and EBNA3C, in contrast to its effect at their protein levels. Additionally, in agreement to the previously published data, our results also showed a similar trend of EBV lytic cycle activation in both proteasome inhibitors and NaBu/TPA treated LCLs as compared to the control cells (Fig. 11B, D, F, H).

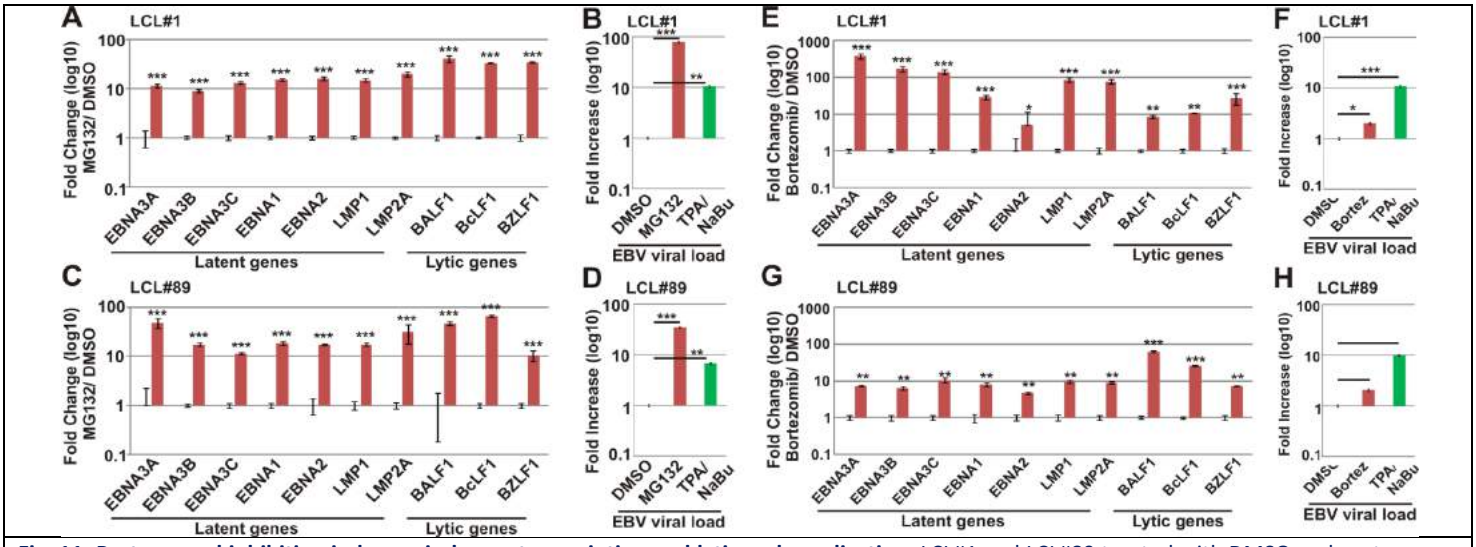

Fig. 11: Proteasomal inhibition induces viral gene transcription and lytic cycle replication. LCL#1 and LCL#89 treated with DMSO and proteasome inhibitors - (A-D) MG132 or (E-H) bortezomib were subjected to real-time PCR analyses for (A, C, E, G) viral transcripts or (B, D, F, H) viral DNA. (B, D, F, H) LCLs were treated with NaBu/**TPA** for 24 h to induce viral lytic cycle as positive control.

Proteasome inhibitors can be used as potential therapeutic strategy against EBV associated B-cell lymphomas, where EBNA3C is expressed: Proteasome inhibitors specifically inhibit degradation of poly-ubiquitinated proteins through UPS, resulting in the stabilization of several tumor suppressor proteins that eventually promote cell-cycle arrest and apoptosis [31][32]. Induction of viral lytic replication in EBV transformed B-lymphocytes together with EBNA3C degradation upon proteasomal inhibition prompted us to evaluate proteasome inhibitors as a potential therapeutic strategy against EBV associated B-cell lymphomas where EBNA3C is expressed, particularly those are generated in an immunocompromised background.

Soft agar based colony formation assays and cell viability experiments using trypan blue exclusion method on two LCLs (LCL#1 and LCL#89) demonstrated that both laboratory based and clinically approved proteasome inhibitors, MG132 and bortezomib, respectively, caused a significant reduction of total number of viable cells and colony formation ability in a dose dependent manner (Fig. 12A–D). Bortezomib (LD50: ~0.5 µM) showed approximately 10 fold higher cytotoxity than that of MG132 (LD50: ~5 µM) in LCLs (Fig. 12D). To determine whether proteasomal inhibition caused apoptotic cell death, LCLs either left untreated (DMSO control) or treated with both MG132 (5 µM) and bortezomib (0.5 µM) for 24 h were stained with FITC labeled Annexin V in combination with propidium iodide (PI) and subjected for apoptosis analyses (Fig. 12E). The results demonstrated that proteasome inhibition significantly induced apoptotic cell death in both LCLs (Fig. 12E).

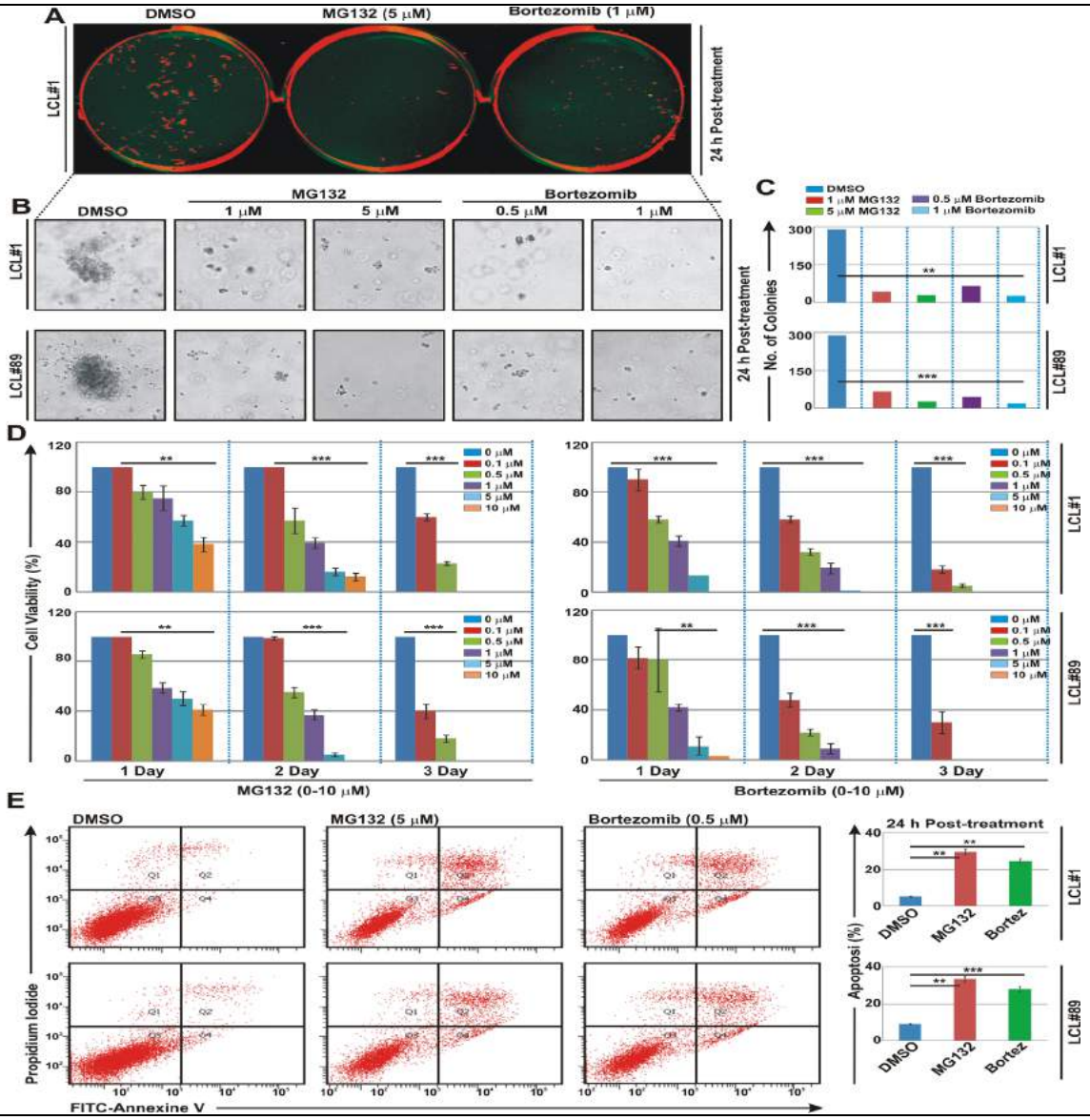

Fig. 12: Proteasome inhibitors can be used as potential therapeutic strategy against EBV associated B-cell lymphomas. (A-C) LCLs were treated with increasing concentrations of MG132 or bortezomib for 24 h and subjected for (A-C) soft agar colony formation assay and (D) cell viability assay by Trypan blue exclusion method using an automated cell counter. (E) LCLs treated with 5 µM MG132 or 0.5 µM bortezomib were subjected to apoptosis assay using annexin V/propidium iodide (PI) staining.

To determine whether proteasome inhibitors may exert different cytotoxic effects on B-cell lymphomas in respect to EBV infection status, cell viability assays was conducted in two EBV negative (BJAB and DG75) and two EBV positive (Namalwa and Raji) BL lines (Fig. 13A). The results demonstrated that EBV positive lines both EBNA3C positive Namalwa and EBNA3C negative Raji cells as compared to EBV negative lines were somewhat more sensitive (~2 fold) to proteasome inhibitors induced cell death (Fig. 13A), while an opposing effect was observed for autophagy inhibitors (Fig. 13B). A similar trend of cell death in both EBNA3C negative line Raji and EBNA3C positive line Namalwa in response to proteasomal inhibition could possibly due to induction of viral lytic replication promoted by proteasome inhibitors as observed in LCLs (Fig. 12D). EBNA3C expression was checked in different cell lines used in this study by western blot analyses (Fig. 13C).

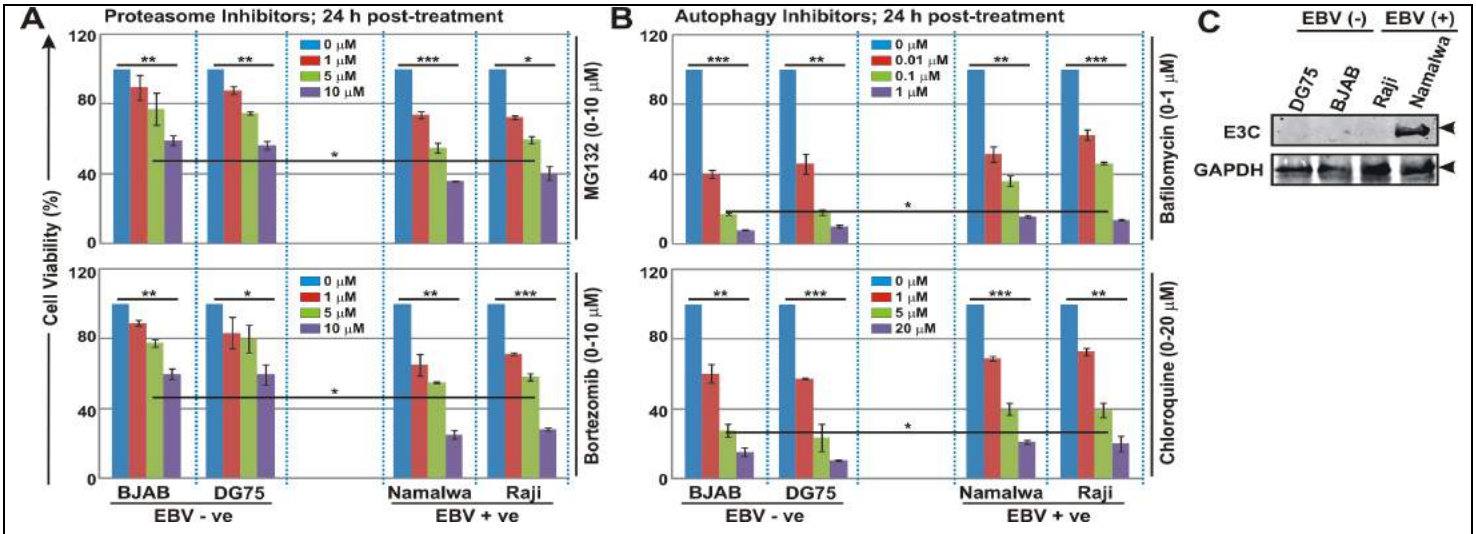

Fig. 13. Effect of proteasomal and lysosomal inhibitors on EBV positive and negative B-cell lymphoma cells. (A-B) ~0.5 × 10^5 cells were plated with indicated drugs. Cell viability was measured by using Trypan blue method. (C)~10 x 10^6 cells were harvested, lysed in RIPA buffer and subjected to western blot analyses with anti-GAPDH (as loading control) and anti-EBNA3C antibodies. Error bars represent standard deviations of duplicate assays of two independent experiments. *, **, *** = p-value < 0.01, 0.005 and 0.001 respectively.

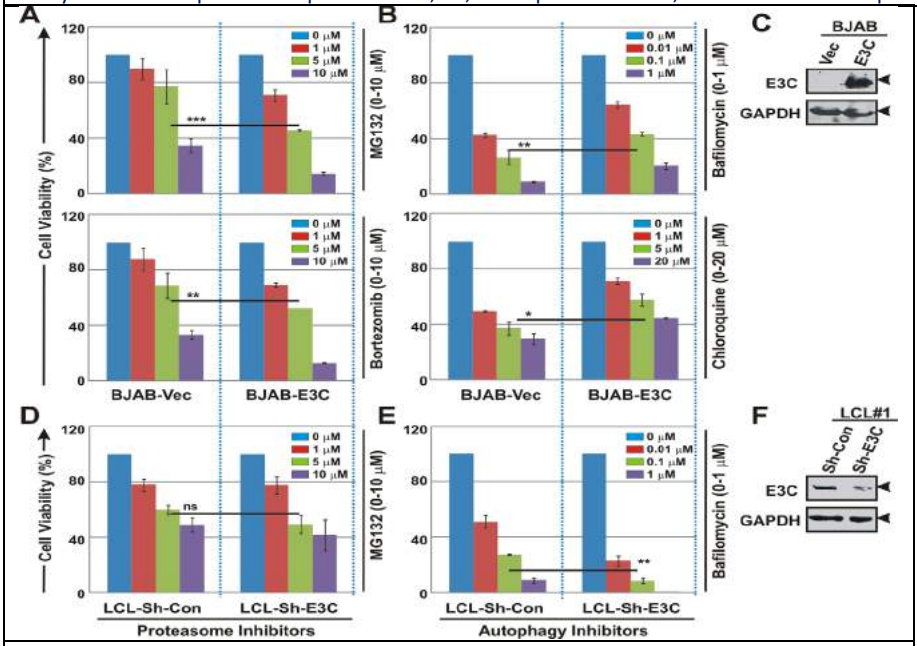

Fig. 14. EBNA3C expressing cells are sensitive towards proteasome inhibitors but not to autophagy inhibitors. (A-B and D-E) ~0.5 × 10^5 cells were plated with indicated drugs. Cell viability was measured by using Trypan blue method. (C and F) ~10 x 10^6 cells were harvested, lysed in RIPA buffer and subjected to western blot analyses with anti-GAPDH (as loading control) and anti-EBNA3C antibodies. Error bars represent standard deviations of duplicate assays of two independent experiments. *, **, *** = p-value < 0.01, 0.005 and 0.001 respectively.

EBNA3C expressing B-cells are more sensitive to apoptotic cell death induced by proteasome inhibitors: Recently our lab has demonstrated that EBNA3C expression in EBV transformed B-lymphocytes significantly protects cell death induced by autophagy inhibitors [18]. Since EBNA3C was shown to enhance cytoprotective autophagy as well as block apoptosis in response to several cellular insults, similar cell viability assays were carried out in both EBNA3C stably expressing BJAB cells and EBNA3C knockdown LCLs to specifically determine if EBNA3C expression may influence proteasome inhibitors mediated cell death (Figs. 14A and 15A). The results demonstrated that while EBNA3C expressing B-cells as compared to the control line were more susceptible to cell-death induced by proteasome inhibitors in a dose dependent fashion, EBNA3C expression as expected led to a significant

protection to cell death caused by autophagy inhibitors (Fig. 14A-B and 15A). EBNA3C knockdown in LCLs reversed the effect of both proteasome and autophagy inhibitors (Fig. 14D-E). EBNA3C stable expression in BJAB and knockdown in LCLs were checked by western blot analyses (Figs. 14C and 14F Fig, respectively).

Susceptibility of proteasomal inhibitors mediated cell death in EBNA3C expressing B-cells was further investigated by apoptosis, PARP cleavage and soft agar colony formation assays (Fig. 15B-D). The results confirmed that EBNA3C expression led to increased cell apoptosis, PARP cleavage and reduced colony formation ability in response to both proteasome inhibitors (Fig. 15B, 15C and 15D, respectively) as compared to control cells. Overall, the data show promise for proteasome inhibitors as anti-cancer drugs against EBV associated B-cell lymphomas where EBNA3C is expressed (Fig. 16).

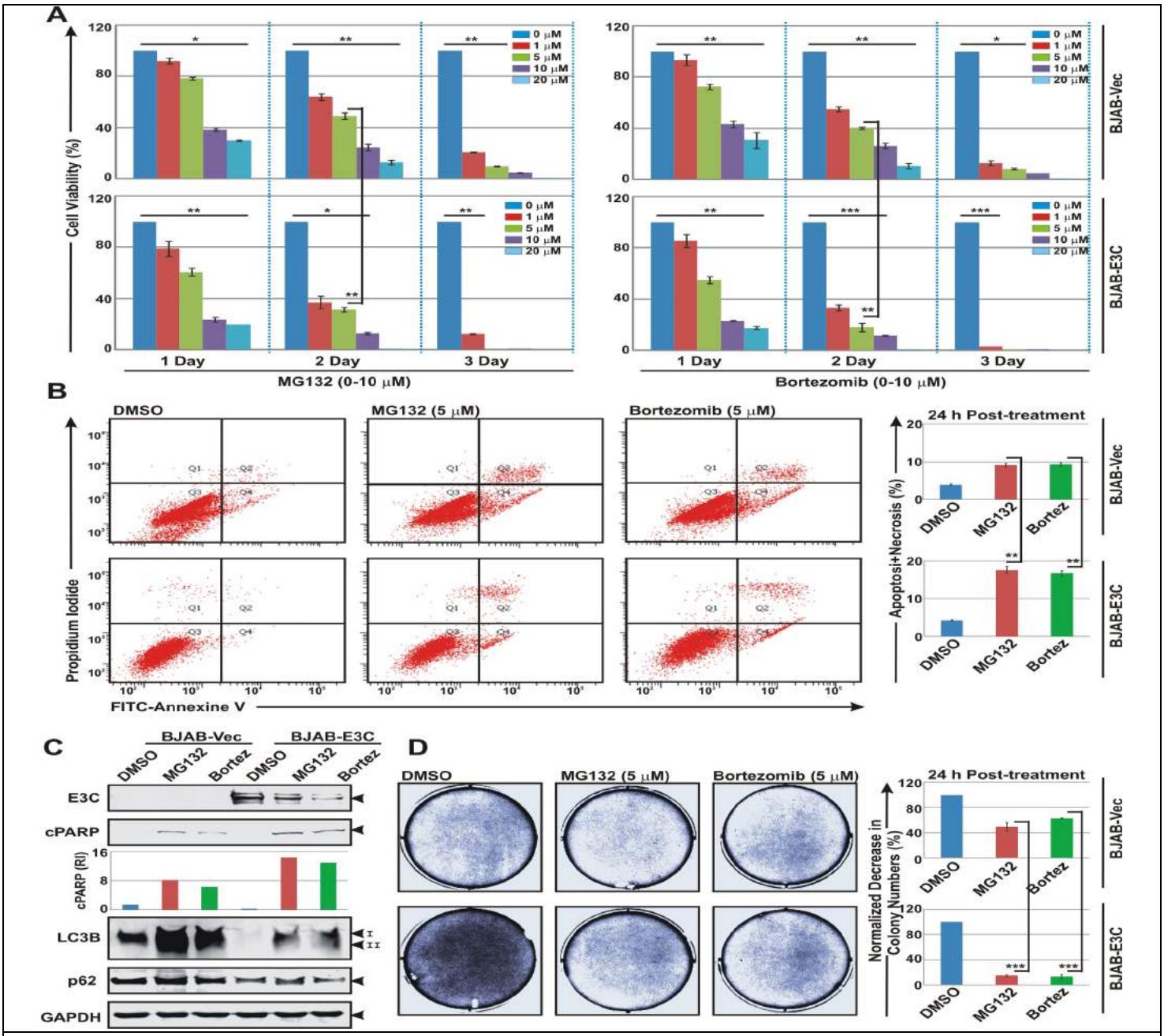

Fig. 15. EBNA3C expressing B-cells are more sensitive to apoptotic cell death induced by proteasome inhibitors. (A) ~0.5 × 105 BJAB cells stably harboring vector or EBNA3C expressing plasmid plated into each well of six-well plates were either left untreated (DMSO control) or treated with increasing concentrations (0-20 μM) of MG132 or bortezomib for 3 days. Viability was measured by Trypan blue exclusion method. (B-D) ~10 × 105 BJAB-vector or BJAB-EBNA3C cells were treated with DMSO, or 5 μM of MG132 or bortezomib for 24 h were subjected to (B) apoptosis assay using annexin V/propidium iodide (PI) staining, (C) For western blot analyses GAPDH blot was used as loading control in western blot analyses. Protein bands were quantified by Odyssey imager software and indicated as bar diagrams at the bottom of corresponding lanes. Error bars represent standard deviations of duplicate assays of two independent experiments. *, **, *** = p-value < 0.01, 0.005 and 0.001 respectively.

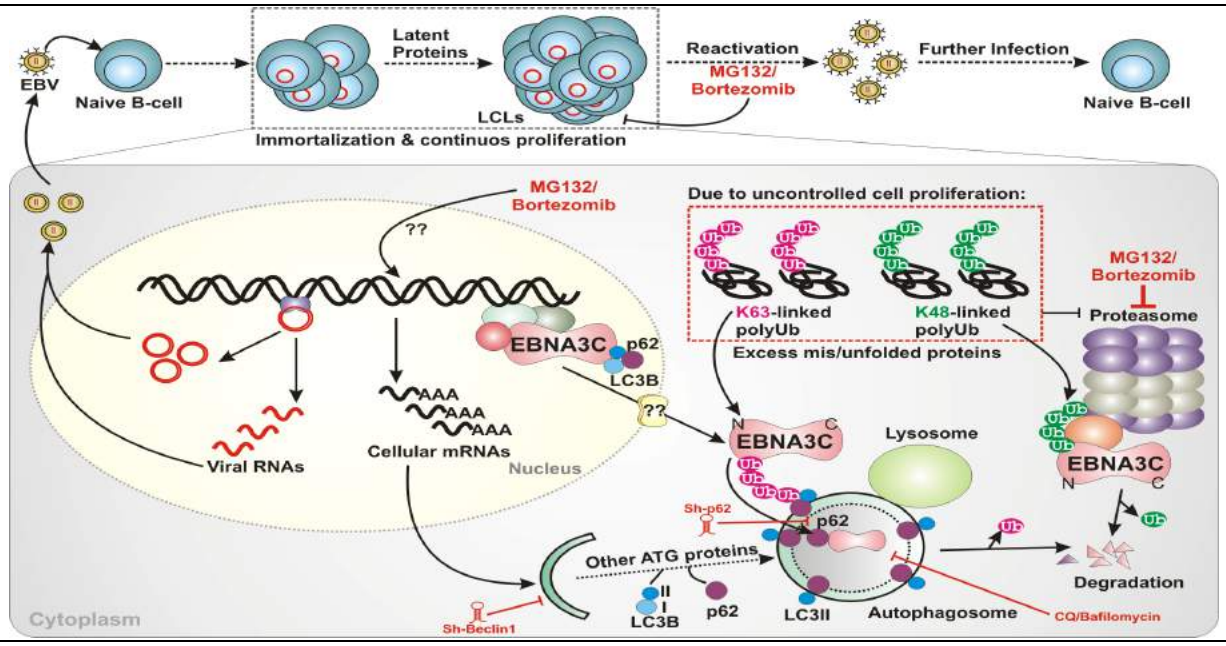

Fig. 16: Schematic representation of proteasomal inhibition mediated EBNA3C's degradation.

Conclusion:

- EBV encoded EBNA3 family proteins are specifically expressed in EBV induced B-cell lymphomas generated in an immunocompromised background. Although these proteins are in general extremely stable in growing EBV induced B-lymphocytes, our results evidently demonstrated that proteasomal inhibition leads to degradation of EBNA3 family members — specifically two EBV essential oncoproteins EBNA3A and EBNA3C, but not the viral tumor suppressor protein EBNA3B.
- RNA-Seq data reveals that proteasomal inhibition elevates transcription of several autophagy genes involved in autophagosme formation, while it leads to a drastic reduction of mRNA levels of genes particularly involved in DNA replication and nucleosome assembly.
- Autophagy stimulated by proteasomal inhibition is required for the degradation of EBNA3C. Beclin 1 knockdown using specific sh-RNA or lysosomal inhibition by chemical inhibitors – bafilomycin or chloroquine treatment partially rescue EBNA3C degradation triggered by proteasomal inhibition in EBV transformed B-lymphocytes. This is the first report describing that a viral oncoprotein is targeted for autophagy mediated degradation in response to proteasomal inhibition.
- EBNA3C interacts and colocalizes with p62-LC3B complex in the cytoplasmic fraction when proteasome is compromised. p62/SQSTM1 knockdown significantly reverses the EBNA3C degradation phenomenon in the presence of proteasomal inhibitor.
- EBNA3C is predominantly K63-linked polyubiquitinated when proteasome is inhibited. In contrast to K48-linked polyubiquitination, together with EBNA3C, K63-linked polyubiquitination level is notably decreased in MG132 treated LCLs, indicating that K63-linked polyubiquitinated substrates (including EBNA3C) are recycled in autophagy-lysosomal pathway, when proteasome is inhibited.
- N-terminal domain of EBNA3C, specifically first 50 residues containing PEST sequence, is important for autophagy mediated degradation in response to proteasomal inhibition.
- EBNA3C N-terminal domain is degraded in the both nuclear and cytoplsamic fractions upon proteasomal inhibition. Putative nuclear export signal (NES) residing at both N- terminal and C-terminal domains play a crucial role for EBNA3C degradation in the cytoplasm through autophagy mechanism when proteasome is inhibited or overloaded due to accumulation of mis-/un-folded proteins. N-terminal domain of EBNA3C participates within p62-LC3B complex and thus plays a critical role in EBNA3C degradation.
- Proteasomal inhibition induces both viral lytic and latent gene transcription, which ultimately leads to EBV lytic cycle activation. This allows us to consider a new promising therapeutic approach of using proteasome inhibitors (viz. bortezomib) in combination with EBV replication inhibitors (viz. Ganciclovir) for patients affected with EBV induced B-cell lymphomas.

- Proteasome inhibitors can cause apoptotic cell death in EBV transformed LCLs in a dose dependent fashion. EBV positive lines as compared to EBV negative lines are somewhat more sensitive (~2 fold) to proteasome inhibitors induced cell death, in contrast to autophagy inhibitors.
- EBNA3C expressing B-cells are more sensitive to apoptotic cell death induced by proteasome inhibitors. Overall, the data show promise for proteasome inhibitors as anti-cancer drugs against multiple EBV associated B-cell lymphomas where EBNA3C is expressed.

Table-1: List of primers used in qPCR analysis

Gene Name	Ref. Sequences	Primer Sequences
EBNA3A	YP_401669.1	Fw- 5'-GCCCTGGATGACAACATGGA-3'; Rv- 5'-CAGGTGGGCATCTTCTGCTT-3'
EBNA3B	NC_007605.1	Fw- 5'-CCCTTGCGGATGCAGCCAAT-3'; Fw- 5'-GGCTGATATGGAATGTGCCC-3'
EBNA3C	YP_401671.1	Fw- 5'-AAGGTGCATTTACCCCACTG-3'; Rv- 5'-AGCAGTAGCTTGGGAACACC-3'
EBNA3A*	YP_401669.1	Fw- 5'-CTAAGAACACTTCTTCAAGC-3'; Rv- 5'-CTCGGTATTTGAAATCTGG-3'
EBNA3B*	NC_007605.1	Fw- 5'-GGGATCTGAGCCTATTTCAC-3'; Fw- 5'-TTCCAACGCCTCTGCTTAAC-3'
EBNA3C*	YP_401671.1	Fw- 5'-GACATCACACCATATACCGC-3'; Rv- 5'-TGTTAGAAGCCAATGTCGCC-3'
EBNA1	YP_401677.1	Fw- 5'-CATTGAGTCGTCTCCCCTTTGGAAT-3'; Rv- 5'-TCATAACAAGGTCCTTAATCGCATC-3'
EBNA2	YP_401644.1	Fw- 5'-GAGACCAGAGCCAAACACCTCCAGT-3'; Rv- 5'-TTAGGGGTTGCCGTGTGTGAATTTC-3'
LMP1	YP_401722.1	Fw- 5'-CCCGCACCCTCAACAAGCTACCGAT-3'; Rv- 5'-TTGTCAGGACCACCTCCAGGTGCGC-3'
LMP2A	YP_401631.1	Fw- 5'-CTCTCACTTCTACTCTTGGCAG-3'; Rv- 5'-AGTCAAACGGCGCCATCTCCTT-3'
BALF1	YP_401718	Fw- 5'-GCTGGCCTTGAGGGCGCTGAGGACT-3'; Rv- 5'-CACCCACGGAAGCCCTCTGGACTTC-3'
BCLF1	YP_401697.1	Fw- 5'-CCTCTTGGAATGCAGCTGGGGCCAG-3'; Rv- 5'-CCAATTATGACCTGCTGCGGCTGGA-3'
BZLF1	YP_401673.1	Fw- 5'- CCAGGTTGAGGTGCTTCTCCCCCGG-3'; Rv- 5'-AACCGCTCCGACTGGGTCGTGGTTT-3'
MAP1LC3B	NM_022818	Fw- 5'-AAGCTGCTTCTCACCCTTGT-3'; Rv- 5'-GAGAAGACCTTCAAGCAGCG-3'
SQSTM1	NM_003900	Fw- 5'-TTCTTTTCCCTCCGTGCTC-3'; Rv- 5'-GGATCCGAGTGTGAATTTCC-3'
GABARAPL1	NM_031412.4	Fw- 5'-GGTGCATCATGAAGTTCCAG-3'; Rv- 5'-GGCTTTTGGAGCCTTCTCTA-3'
CTSD	NM_001909.5	Fw- 5'-AGCCCTCCAGCCTTCTG-3'; Rv- 5'-CGGATGGACGTGAACTTGT-3'
HSPA8	NM_006597.6	Fw- 5'-TATTGGAGCCAGGCCTACAC-3'; Rv- 5'-AGTGGTTCGGTTTCCCTGAT-3'
HSP90AA1	NM_001017963.3	Fw- 5'-GGTCCTGTGCGGTCACTTAG-3'; Rv- 5'-AAAGGCGAACGTCTCAACC-3'
GAPDH	NM_001289745.3	Fw- 5'-AATGAAGGGGTCATTGATGG-3'; Rv- 5'-AAGGTGAAGGTCGGAGTCAA-3'
B2M	NM_004048.3	Fw- 5'-GAGGCTATCCAGCGTACTCCA-3'; Rv- 5'-CGGCAGGCATACTCATCTTTT-3'
RPLPO	NM_007475.5	Fw- 5'-ATCTGCTTGGAGCCCACAT-3'; Rv- 5'-GCGACCTGGAAGTCCAACTA-3'

Reference:

[1] Y. T. Kwon and A. Ciechanover, "The Ubiquitin Code in the Ubiquitin-Proteasome System and Autophagy," *Trends in Biochemical Sciences*. 2017, doi: 10.1016/j.tibs.2017.09.002.

[2] A. Lilienbaum, "Relationship between the proteasomal system and autophagy.," *Int. J. Biochem. Mol. Biol.*, vol. 4, no. 1, pp. 1–26, 2013.

[3] A. M. Burger and A. K. Seth, "The ubiquitin-mediated protein degradation pathway in cancer: therapeutic implications," *Eur. J. Cancer*, vol. 40, no. 15, pp. 2217–2229, 2004, doi: https://doi.org/10.1016/j.ejca.2004.07.006.

[4] S. H. Lecker, A. L. Goldberg, and W. E. Mitch, "Protein Degradation by the Ubiquitin{\textendash}Proteasome Pathway in Normal and Disease States," *J. Am. Soc. Nephrol.*, vol. 17, no. 7, pp. 1807–1819, 2006, doi: 10.1681/ASN.2006010083.

[5] V. Kirkin, D. G. McEwan, I. Novak, and I. Dikic, "A Role for Ubiquitin in Selective Autophagy," *Molecular Cell*. 2009, doi: 10.1016/j.molcel.2009.04.026.

[6] V. Cohen-Kaplan *et al.*, "p62- and ubiquitin-dependent stress-induced autophagy of the mammalian 26S proteasome," *Proc. Natl. Acad. Sci.*, 2016, doi: 10.1073/pnas.1615455113.

[7] F. Ohtake, H. Tsuchiya, Y. Saeki, and K. Tanaka, "K63 ubiquitylation triggers proteasomal degradation by

seeding branched ubiquitin chains," *Proc. Natl. Acad. Sci.*, vol. 115, no. 7, pp. E1401--E1408, 2018, doi: 10.1073/pnas.1716673115.
[8] S. Manohar *et al.*, "Polyubiquitin Chains Linked by Lysine Residue 48 (K48) Selectively Target Oxidized Proteins In Vivo.," *Antioxid. Redox Signal.*, vol. 31, no. 15, pp. 1133–1149, Nov. 2019, doi: 10.1089/ars.2019.7826.
[9] M. A. EPSTEIN, B. G. ACHONG, and Y. M. BARR, "VIRUS PARTICLES IN CULTURED LYMPHOBLASTS FROM BURKITT'S LYMPHOMA.," *Lancet (London, England)*, vol. 1, no. 7335, pp. 702–703, Mar. 1964, doi: 10.1016/s0140-6736(64)91524-7.
[10] G. Niedobitek, N. Meru, and H. Delecluse, "Epstein-Barr virus infection and human malignancies," *Int J Exp Pathol*, 2001.
[11] D. J. Moss, S. R. Burrows, S. L. Silins, I. Misko, and R. Khanna, "The immunology of Epstein-Barr virus infection," *Philos Trans R Soc L. B Biol Sci*, 2001.
[12] J. Hui-Yuen, S. McAllister, S. Koganti, E. Hill, and S. Bhaduri-McIntosh, "Establishment of Epstein-Barr Virus Growth-transformed Lymphoblastoid Cell Lines," *J. Vis. Exp.*, 2011, doi: 10.3791/3321.
[13] A. Saha and E. S. Robertson, "Epstein-barr virus-associated B-cell lymphomas: Pathogenesis and clinical outcomes," *Clinical Cancer Research*. 2011, doi: 10.1158/1078-0432.CCR-10-2578.
[14] S. Bhattacharjee, S. G. Roy, P. Bose, and A. Saha, "Role of EBNA-3 family proteins in EBV associated B-cell lymphomagenesis," *Frontiers in Microbiology*. 2016, doi: 10.3389/fmicb.2016.00457.
[15] S. Maruo, Y. Wu, T. Ito, T. Kanda, E. D. Kieff, and K. Takada, "Epstein-Barr virus nuclear protein EBNA3C residues critical for maintaining lymphoblastoid cell growth," *Proc. Natl. Acad. Sci.*, vol. 106, no. 11, pp. 4419–4424, 2009, doi: 10.1073/pnas.0813134106.
[16] J. S. Knight, N. Sharma, and E. S. Robertson, "SCFSkp2 complex targeted by Epstein-Barr virus essential nuclear antigen.," *Mol. Cell. Biol.*, 2005, doi: 10.1128/MCB.25.5.1749-1763.2005.
[17] R. Touitou, J. O'Nions, J. Heaney, and M. J. Allday, "Epstein-Barr virus EBNA3 proteins bind to the C8/α7 subunit of the 20S proteasome and are degraded by 20S proteasomes in vitro, but are very stable in latently infected B cells," *J. Gen. Virol.*, 2005, doi: 10.1099/vir.0.80763-0.
[18] S. Bhattacharjee *et al.*, "Transcriptional and epigenetic modulation of autophagy promotes EBV oncoprotein EBNA3C induced B-cell survival," *Cell Death Dis.*, vol. 9, no. 6, p. 605, 2018, doi: 10.1038/s41419-018-0668-9.
[19] S. Ito, "Proteasome Inhibitors for the Treatment of Multiple Myeloma," *Cancers (Basel).*, vol. 12, no. 2, p. 265, Jan. 2020, doi: 10.3390/cancers12020265.
[20] S. Gandolfi, J. P. Laubach, T. Hideshima, D. Chauhan, K. C. Anderson, and P. G. Richardson, "The proteasome and proteasome inhibitors in multiple myeloma.," *Cancer Metastasis Rev.*, vol. 36, no. 4, pp. 561–584, Dec. 2017, doi: 10.1007/s10555-017-9707-8.
[21] H. Vakifahmetoglu-Norberg *et al.*, "Chaperone-mediated autophagy degrades mutant p53," *Genes Dev.*, vol. 27, no. 15, pp. 1718–1730, Aug. 2013, doi: 10.1101/gad.220897.113.
[22] M. Halasi, B. Pandit, and A. L. Gartel, "Proteasome inhibitors suppress the protein expression of mutant p53," *Cell Cycle*, vol. 13, no. 20, pp. 3202–3206, 2014, doi: 10.4161/15384101.2014.950132.
[23] S. P. Yenamandra, R. Sompallae, G. Klein, and E. Kashuba, "Comparative analysis of the Epstein-Barr virus encoded nuclear proteins of EBNA-3 family.," *Comput. Biol. Med.*, vol. 39, no. 11, pp. 1036–1042, Nov. 2009, doi: 10.1016/j.compbiomed.2009.08.006.
[24] P. Xu *et al.*, "Quantitative proteomics reveals the function of unconventional ubiquitin chains in proteasomal degradation.," *Cell*, vol. 137, no. 1, pp. 133–145, Apr. 2009, doi: 10.1016/j.cell.2009.01.041.
[25] M. L. Seibenhener, J. R. Babu, T. Geetha, H. C. Wong, N. R. Krishna, and M. W. Wooten, "Sequestosome 1/p62 is a polyubiquitin chain binding protein involved in ubiquitin proteasome degradation.," *Mol. Cell. Biol.*, vol. 24, no. 18, pp. 8055–8068, Sep. 2004, doi: 10.1128/MCB.24.18.8055-8068.2004.
[26] M. Cabe, D. J. Rademacher, A. B. Karlsson, S. Cherukuri, and J. C. Bakowska, "PB1 and UBA domains of

p62 are essential for aggresome-like induced structure formation.," *Biochem. Biophys. Res. Commun.*, vol. 503, no. 4, pp. 2306–2311, Sep. 2018, doi: 10.1016/j.bbrc.2018.06.153.
[27] H. Li, J. Hu, X. Luo, A. M. Bode, Z. Dong, and Y. Cao, "Therapies based on targeting Epstein-Barr virus lytic replication for EBV-associated malignancies.," *Cancer Sci.*, vol. 109, no. 7, pp. 2101–2108, Jul. 2018, doi: 10.1111/cas.13634.
[28] H. Cen and J. L. McKnight, "EBV-immortalized isogenic human B-cell clones exhibit differences in DNA-protein complex formation on the BZLF1 and BRLF1 promoter regions among latent, lytic and TPA-activated cell lines.," *Virus Res.*, vol. 31, no. 1, pp. 89–107, Jan. 1994, doi: 10.1016/0168-1702(94)90073-6.
[29] E. M. Westphal, W. Blackstock, W. Feng, B. Israel, and S. C. Kenney, "Activation of lytic Epstein-Barr virus (EBV) infection by radiation and sodium butyrate in vitro and in vivo: a potential method for treating EBV-positive malignancies.," *Cancer Res.*, vol. 60, no. 20, pp. 5781–5788, Oct. 2000.
[30] C. M. Shirley *et al.*, "Bortezomib induction of C/EBPβ mediates Epstein-Barr virus lytic activation in Burkitt lymphoma," *Blood*, vol. 117, no. 23, pp. 6297–6303, Jun. 2011, doi: 10.1182/blood-2011-01-332379.
[31] D. Wang *et al.*, "Proteasome inhibition boosts autophagic degradation of ubiquitinated-AGR2 and enhances the antitumor efficiency of bevacizumab," *Oncogene*, vol. 38, no. 18, pp. 3458–3474, 2019, doi: 10.1038/s41388-019-0675-z.
[32] L. J. Crawford, B. Walker, and A. E. Irvine, "Proteasome inhibitors in cancer therapy.," *J. Cell Commun. Signal.*, vol. 5, no. 2, pp. 101–110, Jun. 2011, doi: 10.1007/s12079-011-0121-7.

Publications:

1. **Gain C**, Malik S, Bhattacharjee S, Ghosh A, Robertson ES, Das BB, Saha A. **PLoS Pathog.** 2020 Feb 24;16(2):e1008105. doi: 10.1371/journal.ppat.1008105. Proteasomal inhibition triggers viral oncoprotein degradation via autophagy-lysosomal pathway.
2. **Gain C**, Sarkar A, Bural S, Rakshit M, Banerjee J, Dey A, Biswas N, Kar GK, Saha A. **Bioorg Med Chem.** 2021 May 1;37:116112. doi: 10.1016/j.bmc.2021.116112. Identification of two novel thiophene analogues as inducers of autophagy mediated cell death in breast cancer cells.
3. Bhattacharjee S, Bose P, Patel K, Roy SG, **Gain C**, Gowda H, Robertson ES, Saha A. **Cell Death Dis.** 2018 May 22;9(6):605. doi: 10.1038/s41419-018-0668-9. Transcriptional and epigenetic modulation of autophagy promotes EBV oncoprotein EBNA3C induced B-cell survival.
4. **Gain C**, Saha A. Modulation of autophagy in human gammaherpes virus induced malignancies (Review manuscript in progress).

Presentation at academic conferences/meetings:

1. **Gain C**, Malik S, Bhattacharjee S, Ghosh A, Robertson ES, Das BB, Saha A. "Proteasomal Inhibition Triggers Viral Oncoprotein Degradation via Autophagy-Lysosomal Pathway". **Poster presentation** in International Conference on Autophagy and Lysosomes 2020 from January 16-18, 2020 at IISC, Bengaluru.
2. **Gain C**, Malik S, Bhattacharjee S, Ghosh A, Robertson ES, Das BB, Saha A. "Proteasomal Inhibition Enhances Viral Protein Degradation via Autophagy-Lysosomal Pathway." **Poster presentation** in 6th Molecular Virology Meeting 2019 from 28th Feb- 2nd March, 2019 at School of Bioscience at IIT Kharagpur.
3. Bhattacharjee S, Bose P, Ghosh Roy S, **Gain C**, Saha A. "Epstein - Barr Virus Nuclear Antigen EBNA3C Transcriptionally Modulates Autophagy Network- A Clue to B- cell Lymphomagenesis". **Poster presentation** in '19th Transcription Assembly Meeting' from November 8-9, 2016 at Bose Institute, Kolkata.

PLOS PATHOGENS

RESEARCH ARTICLE

Proteasomal inhibition triggers viral oncoprotein degradation via autophagy-lysosomal pathway

Chandrima Gain[1], Samaresh Malik[1], Shaoni Bhattacharjee[1], Arijit Ghosh[2], Erle S. Robertson[3], Benu Brata Das[2], Abhik Saha[1]*

1 Department of Life Sciences, Presidency University, West Bengal, India, **2** Laboratory of Molecular Biology, School of Biological Sciences, Indian Association for the Cultivation of Science, Jadavpur, Kolkata, India, **3** Department of Otorhinolaryngology Head and Neck Surgery, and the Tumor Virology Program, Abramson Comprehensive Cancer Center, Perelman School of Medicine at the University of Pennsylvania, Philadelphia, Pennsylvania, United States of America

* abhik.dbs@presiuniv.ac.in

Check for updates

OPEN ACCESS

Citation: Gain C, Malik S, Bhattacharjee S, Ghosh A, Robertson ES, Das BB, et al. (2020) Proteasomal inhibition triggers viral oncoprotein degradation via autophagy-lysosomal pathway. PLoS Pathog 16(2): e1008105. https://doi.org/10.1371/journal.ppat.1008105

Editor: Robert F. Kalejta, University of Wisconsin-Madison, UNITED STATES

Received: September 15, 2019

Accepted: January 28, 2020

Published: February 24, 2020

Copyright: © 2020 Gain et al. This is an open access article distributed under the terms of the Creative Commons Attribution License, which permits unrestricted use, distribution, and reproduction in any medium, provided the original author and source are credited.

Data Availability Statement: All relevant data are within the manuscript and its Supporting Information files.

Funding: E.S.R. is a scholar of the Leukemia and Lymphoma Society of America. A.S. and B.B.D. are Wellcome Trust/DBT India Alliance Intermediate Fellows. C.B. and S.M. are the recipients of UGC-NET Senior and Junior Research Fellowship, respectively, India. S.B. is recipient of DST-Inspire Senior Research Fellowship and A.G. is recipient of CSIR-NET Senior Research Fellowship. This work

Abstract

Epstein-Barr virus (EBV) nuclear oncoprotein EBNA3C is essential for B-cell transformation and development of several B-cell lymphomas particularly those are generated in an immuno-compromised background. EBNA3C recruits ubiquitin-proteasome machinery for deregulating multiple cellular oncoproteins and tumor suppressor proteins. Although EBNA3C is found to be ubiquitinated at its N-terminal region and interacts with 20S proteasome, the viral protein is surprisingly stable in growing B-lymphocytes. EBNA3C can also circumvent autophagy-lysosomal mediated protein degradation and subsequent antigen presentation for T-cell recognition. Recently, we have shown that EBNA3C enhances autophagy, which serve as a prerequisite for B-cell survival particularly under growth deprivation conditions. We now demonstrate that proteasomal inhibition by MG132 induces EBNA3C degradation both in EBV transformed B-lymphocytes and ectopic-expression systems. Interestingly, MG132 treatment promotes degradation of two EBNA3 family oncoproteins–EBNA3A and EBNA3C, but not the viral tumor suppressor protein EBNA3B. EBNA3C degradation induced by proteasomal inhibition is partially blocked when autophagy-lysosomal pathway is inhibited. In response to proteasomal inhibition, EBNA3C is predominantly K63-linked polyubiquitinated, colocalized with the autophagy-lysosomal fraction in the cytoplasm and participated within p62-LC3B complex, which facilitates autophagy-mediated degradation. We further show that the degradation signal is present at the first 50 residues of the N-terminal region of EBNA3C. Proteasomal inhibition reduces the colony formation ability of this important viral oncoprotein, induces apoptotic cell death and increases transcriptional activation of both latent and lytic gene expression which further promotes viral reactivation from EBV transformed B-lymphocytes. Altogether, this study offers rationale to use proteasome inhibitors as potential therapeutic strategy against multiple EBV associated B-cell lymphomas, where EBNA3C is expressed.

Bioorganic & Medicinal Chemistry xxx (xxxx) 116112

Contents lists available at ScienceDirect

Bioorganic & Medicinal Chemistry

journal homepage: www.elsevier.com/locate/bmc

Identification of two novel thiophene analogues as inducers of autophagy mediated cell death in breast cancer cells

Chandrima Gain[a,1], Aparna Sarkar[b,1], Shrea Bural[a,1], Moumita Rakshit[b], Jeet Banerjee[b], Ankita Dey[b], Nabendu Biswas[c], Gandhi K. Kar[b,*], Abhik Saha[a,*]

[a] School of Biotechnology, Presidency University, Second Campus, Plot No. DG/02/02, Premises No. 14-0358, Action Area-ID, New Town, Kolkata 700156, West Bengal, India
[b] Department of Chemistry, Presidency University, 86/1 College Street, Kolkata 700073, West Bengal, India
[c] Department of Life Sciences, Presidency University, 86/1 College Street, Kolkata 700073, West Bengal, India

ARTICLE INFO

Keywords:
Breast cancer
Tanshinones
Thiophene analogues
Autophagy

ABSTRACT

Natural compounds isolated from different medicinal plants remain one of the major resources of anti-cancer drugs due to their enormous chemical diversity. Studies suggested therapeutic potential for various tanshinones, key bioactive lipophilic compounds from the root extracts of *Salvia miltiorrhiza* Bunge, against multiple cancers including breast carcinoma. We designed, synthesized and evaluated anti-cancer properties of a series of condensed and doubly condensed furophenanthraquinones of tanshinone derivatives on two breast cancer lines - MCF7 and MDA-MB-231. We identified two thiophene analogues - compounds **48** and **52** with greater anti-proliferative efficiency (~4 fold) as compared to the natural tanshinones. Mechanistically, we showed that both compounds induced autophagy mediated cell death and partial but significant restoration of cell death in the presence of autophagy inhibitor further supported this notion. Both compounds transcriptionally activated several autophagy genes responsible for autophagosome formation along

Abbreviations: Tan-I, tanshinone-I; Tan-IIA, tanshinone-IIA; NMR, nuclear magnetic resonance; FT-IR, Fourier-transform infrared spectroscopy; TFA, CF_3CO_2H, trifluoroacetic acid; TFAA, $(CF_3CO)_2O$, trifluoroacetic anhydride; $Pd(PPh_3)_4$, tetrakis(triphenylphosphine)palladium(0); Et_3N, triethylamine; DMF, dimethylformamide; hrs, hours; $NaBH_4$, sodium borohydride; EtOH, ethanol; r.t., room temperature; MsCl, methanesulfonyl chloride; LiCl, lithium chloride; KCN, potassium cyanide; Aq., aqueous; KOH, potassium hydroxide; Na_2HPO_4-H_2O, sodium phosphate dibasic; MeOH, methanol; PBr3, phosphorus tribromide; CHCl3, chloroform; atm., atmosphere; DDQ, 2,3-dichloro-5,6-dicyano-1,4-benzoquinone; HRMS, high-resolution mass spectrometry; ESI, electrospray ionization; LC/MS, liquid chromatography–mass spectrometry; MTT, (3-(4, 5-dimethylthiazolyl-2)-2, 5-diphenyltetrazolium bromide); ER, estrogen receptor; PR, progesterone receptor; Her2, human epidermal growth factor receptor 2; DMSO, dimethyl sulfoxide; μM, micromolar; NADPH, nicotinamide adenine dinucleotide phosphate; nm, nanometer; IC_{50}, the concentration that gives half-maximal response; EtBr, ethidium bromide; AO, acridine orange; DNA, deoxyribonucleic acid; PI, propidium iodide; PARP1, poly [ADP-ribose] polymerase 1; Ex, excitation; Em, emission; GAPDH, glyceraldehyde 3-phosphate dehydrogenase; Bcl-2, B-cell lymphoma 2; Bcl-xL, B-cell lymphoma-extra large; BCL2L1, BCL2 like 1; Bim, Bcl-2 interacting mediator of cell death; BCL2L11, BCL2 like 11; Beclin 1, Coiled-Coil, Moesin-Like BCL2-Interacting Protein; Bax, BCL2-associated X, apoptosis regulator; Bak, BCL2-antagonist/killer 1; LC3, microtubule associated protein 1 light chain 3 alpha/beta; p62/SQSTM1, sequestosome 1; ATG, autophagy related gene; PCR, polymerase chain reaction; RNA, ribonucleic acid; ATG16L1, autophagy related 16 like 1; ATG16L2, autophagy related 16 like 2; GABARAP, GABA (Gamma aminobutyric acid) type A receptor-associated protein; GABARAPL1, GABA type A receptor-associated protein like 1; GABARAPL2, GABA type A receptor-associated protein like 2; PIK3CG, phosphatidylinositol-4,5-bisphosphate 3-kinase catalytic subunit gamma; UVRAG, UV radiation resistance associated gene; DDIT3, DNA damage inducible transcript 3; CHOP, C/EBP (CCAAT/enhancer-binding protein)-homologous protein; GADD34, growth arrest and DNA-damage-inducible protein 34; PPP1R15A, protein phosphatase 1 regulatory subunit 15A; PERK, protein kinase R (PKR)-like endoplasmic reticulum kinase; EIF2AK3, eukaryotic translation initiation factor 2 alpha kinase 3; ATF6, activating transcription factor 6; IRE1, inositol-requiring enzyme 1; ERN1, endoplasmic reticulum to nucleus signaling 1; eIF2α, eukaryotic translation initiation factor 2 alpha; ATF4, activating transcription factor 4; cDNA, complementary DNA; ACTB, actin beta; B2M, beta-2-microglobulin; HPRT1, hypoxanthine phosphoribosyltransferase 1; RPLP0, ribosomal protein lateral stalk subunit P0; CQ, choroquine; GFP, green fluorescence protein; mCherry, mFruits family of monomeric red fluorescent proteins (mRFPs); DCM, dichloromethane; Et2O, diethyl ether; P.E, petroleum ether; EtOAc, ethyl acetate; TLC, thin-layer chromatography; H_2SO_4, sulfuric acid; KBr, potassium bromide; $NaHCO_3$, sodium bicarbonate; Na_2SO_4, sodium sulfate; M.P, melting point; QTOF, Quad Time Of Flight; HCl, hydrochloric acid; FITC, fluorescein isothiocyanate

* Corresponding authors.
E-mail addresses: gandhi.chem@presiuniv.ac.in (G.K. Kar), abhik.dbs@presiuniv.ac.in (A. Saha).
[1] Equal Contribution.

https://doi.org/10.1016/j.bmc.2021.116112
Received 14 January 2021; Received in revised form 2 March 2021; Accepted 5 March 2021
0968-0896/© 2021

Bhattacharjee et al. *Cell Death and Disease* (2018)9:605
DOI 10.1038/s41419-018-0668-9

Cell Death & Disease

ARTICLE Open Access

Transcriptional and epigenetic modulation of autophagy promotes EBV oncoprotein EBNA3C induced B-cell survival

Shaoni Bhattacharjee[1], Priyanka Bose[1], Krishna Patel[2], Shatadru Ghosh Roy[1], Chandrima Gain[1], Harsha Gowda[2], Erle S. Robertson[3] and Abhik Saha[1]

Abstract

Epstein-Barr virus (EBV) oncoprotein EBNA3C is indispensable for primary B-cell transformation and maintenance of lymphoblastoid cells outgrowth. EBNA3C usurps two putative cellular pathways—cell-cycle and apoptosis, essentially through modulating ubiquitin-mediated protein-degradation or gene transcription. In cancer cells, these two pathways are interconnected with autophagy,—a survival-promoting catabolic network in which cytoplasmic material including mis/un-folded protein aggregates and damaged organelles along with intracellular pathogens are degraded and recycled in lysosomal compartments. Studies have shown that tumor viruses including EBV can manipulate autophagy as a survival strategy. Here, we demonstrate that EBNA3C elevates autophagy, which serves as a prerequisite for apoptotic inhibition and maintenance of cell growth. Using PCR based micro-array we show that EBNA3C globally accelerates autophagy gene transcription under growth limiting conditions. Reanalyzing the ENCODE ChIP-sequencing data (GSE52632 and GSE26386) followed by ChIP-PCR demonstrate that EBNA3C recruits several histone activation epigenetic marks (H3K4me1, H3K4me3, H3K9ac, and H3K27ac) for transcriptional activation of autophagy genes, notably *ATG3*, *ATG5*, and *ATG7* responsible for autophagosome formation. Moreover, under growth limiting conditions EBNA3C further stimulates the autophagic response through upregulation of a number of tumor suppressor genes, notably cyclin-dependent kinase inhibitors—*CDKN1B* ($p27^{Kip1}$) and *CDKN2A* ($p16^{INK4a}$) and autophagy mediated cell-death modulators—*DRAM1* and *DAPK1*. Together our data highlight a new role of an essential EBV oncoprotein in regulating autophagy cascade as a survival mechanism and offer novel-targets for potential therapeutic expansion against EBV induced B-cell lymphomas.

Introduction

Epstein-Barr virus (EBV) is a lymphotropic gamma-herpesvirus that asymptomatically persists in >95% of the world population[1]. However, in immuno-compromized individuals, the loss of immune-control of the latently-infected B-cells results in the emergence of several B-cell lymphomas[2–4]. In vitro, EBV can efficiently transform resting B-lymphocytes into lymphoblastoid cell-lines (LCLs), providing an excellent model to study EBV-induced B-cell transformation and B-cell lymphomagenesis[5]. In LCLs, EBV expresses six nuclear antigens (EBNAs) and three membrane proteins (LMPs) along with several non-coding RNAs[1,6]. Of these, five viral latent proteins including EBNA2, EBNA3A, EBNA3C, EBNALP, and LMP1 are indispensible for B-cell transformation and subsequent lymphoma development[6,7].

EBNA3C interferes with a number of cellular pathways —most strikingly cell-cycle/apoptosis and ubiquitin-

Correspondence: Abhik Saha (abhik.dbs@presiuniv.ac.in)
[1]Department of Life Sciences, Presidency University, 86/1 College Street, Kolkata 700073 West Bengal, India
[2]Institute of Bioinformatics, Discoverer Building, International Tech Park, Whitefield, Bangalore 560066, India
Full list of author information is available at the end of the article.
These authors contributed equally: Shaoni Bhattacharjee and Priyanka Bose.
Edited by B. Zhivotovsky

© The Author(s) 2018
Open Access This article is licensed under a Creative Commons Attribution 4.0 International License, which permits use, sharing, adaptation, distribution and reproduction in any medium or format, as long as you give appropriate credit to the original author(s) and the source, provide a link to the Creative Commons license, and indicate if changes were made. The images or other third party material in this article are included in the article's Creative Commons license, unless indicated otherwise in a credit line to the material. If material is not included in the article's Creative Commons license and your intended use is not permitted by statutory regulation or exceeds the permitted use, you will need to obtain permission directly from the copyright holder. To view a copy of this license, visit http://creativecommons.org/licenses/by/4.0/.

SPRINGER NATURE CDDpress